The W. M. Keck Observatory Laser Guide Star Adaptive Optics System: Overview

Peter L. Wizinowich, David Le Mignant, Antonin H. Bouchez[1], Randy D. Campbell, Jason C. Y. Chin, Adam R. Contos[2], Marcos A. van Dam, Scott K. Hartman, Erik M. Johansson, Robert E. Lafon

Published 2006 February 9 •

Publications of the Astronomical Society of the Pacific, Volume 118, Number 840

W. M. Keck Observatory, 65-1120 Mamalahoa Highway, Kamuela, HI 96743; peterw@keck.hawaii.edu

Lawrence Livermore National Laboratory, P.O. Box 808, Livermore, CA 94550

[1] Current address: Caltech Optical Observatories, Mail Code 105-24, California Institute of Technology, 1200 East California Boulevard, Pasadena, CA 91125.

[2] Current address: Ball Aerospace, 10 Longs Peak Drive, Broomfield, CO 80021.

[3] Current address: Center for Adaptive Optics, University of California, Santa Cruz, 1156 High Street, Santa Cruz, CA 95064.

Received 2005 September 12
Accepted 2005 October 31
Published 2006 February 9

Peter L. Wizinowich *et al* 2006 *PASP* **118** 297

https://doi.org/10.1086/499290

Abstract

The Keck Observatory began science observations with a laser guide star adaptive optics system, the first such system on an 8–10 m class telescope, in late 2004. This new capability greatly extends the scientific potential of the Keck II Telescope, allowing near–diffraction-limited observations in the near-infrared using natural guide stars as faint as 19th magnitude. This paper describes the conceptual approach and technical implementation followed for this system, including lessons learned, and provides an overview of the early science capabilities.

1. INTRODUCTION

Adaptive optics (AO) systems have been in use on astronomical telescopes since the early 1990s (Graves et al. 1994; Rousset et al. 1994; Rigaut et al. 1998). From the beginning, astronomers recognized the limitations of AO due to the need to use relatively bright stars to measure the wave-front distortions introduced by Earth's atmosphere. To increase the very limited sky coverage of these systems, they have therefore looked for ways to create their own beacons using lasers. The most feasible of these approaches for very large telescopes is to use a sodium-wavelength laser to excite the sodium atoms in Earth's mesosphere (Foy & Labeyrie 1985; Thompson & Gardner 1987). Although experiments with various lasers have been performed at a number of observatories, only a few laser guide star (LGS) based science papers have been published (McCullough et al. 1995; Hackenberg et al. 2000; Perrin et al. 2004), and until recently only the Lick 3 m telescope sodium LGS system has been performing LGS observations on a regular basis (Max et al. 1997). The Lick system was joined in late 2004 by an operational sodium LGS system on the Keck II Telescope.

The W. M. Keck Observatory consists of two 10 m diameter optical/infrared telescopes separated by 85 m, located on the summit of Mauna Kea in Hawaii. Natural guide star (NGS) AO systems have been in operation on the Keck II and Keck I Telescopes since 1999 (Wizinowich et al. 2000a, 2000b) and 2000, respectively. The science instruments behind the AO system have included KCAM, a simple near-infrared imaging engineering camera; NIRSPEC, a near-infrared spectrograph (McLean et al. 1998); NIRC2, a near-infrared camera designed explicitly for AO (K. Matthews et al. 2006, in preparation); an interferometer that combines the light from both telescopes (Colavita et al. 2004); and OSIRIS, an OH-suppression infrared integral field spectrograph (Larkin et al. 2003).

The Keck II AO system was designed from the start to be an LGS system. The laser was fabricated by Lawrence Livermore National Laboratory (LLNL) and delivered in 1998 (Friedman et al. 1998) to a laboratory at Keck headquarters, where it was further engineered by a team of LLNL and Keck personnel. It was integrated with the telescope in 2001 in time for an end-of-the-year first projection of the laser onto the sky. This milestone was followed by continued laser and LGS AO development. The first closed-loop tests with the laser occurred in late 2003. Shared-risk science observations began in late 2004, and 30 LGS AO science nights have been allocated in the second half of 2005.

The nature and limitations of a sodium-wavelength LGS require numerous modifications with respect to an NGS-based AO system. Section 2 discusses these LGS AO issues and the conceptual approaches we chose to address them, as well as the technical implementation of the resulting LGS components. Section 3 describes the laser, associated operational issues, and the laser guide star. We then describe the LGS AO operations, including observing strategy (§ 4) and the early science capabilities (§ 5). Implementing the first LGS AO system on a large telescope has presented numerous challenges, and this paper attempts to share the lessons learned in this process. A separate paper (van Dam et al. 2006) describes the LGS AO system's performance and algorithms in more detail.

2. IMPLEMENTATION

In order to orient the reader, we first provide a schematic of the LGS AO control approach taken in the Keck system. We then review, at a schematic level, the LGS AO issues and the solutions chosen for the Keck system (somewhat as a perspective on historical development). Finally, we describe the physical implementation of the Keck system.

2.1. LGS AO Control

A schematic view of the major Keck LGS AO components is presented in Figure 1. The NGS and LGS light collected by the telescope are reflected off the tip-tilt mirror (TTM), the deformable mirror (DM), and the infrared (IR) transmissive dichroic. The infrared light is transmitted to the science camera. The sodium-wavelength light is transmitted through a sodium-transmissive dichroic to the wave-front sensor (WFS). Since the LGS is not at infinity, it comes to a focus after the NGS focus.

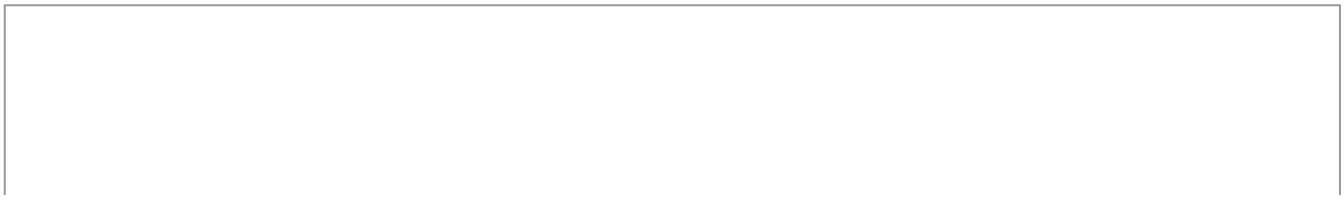

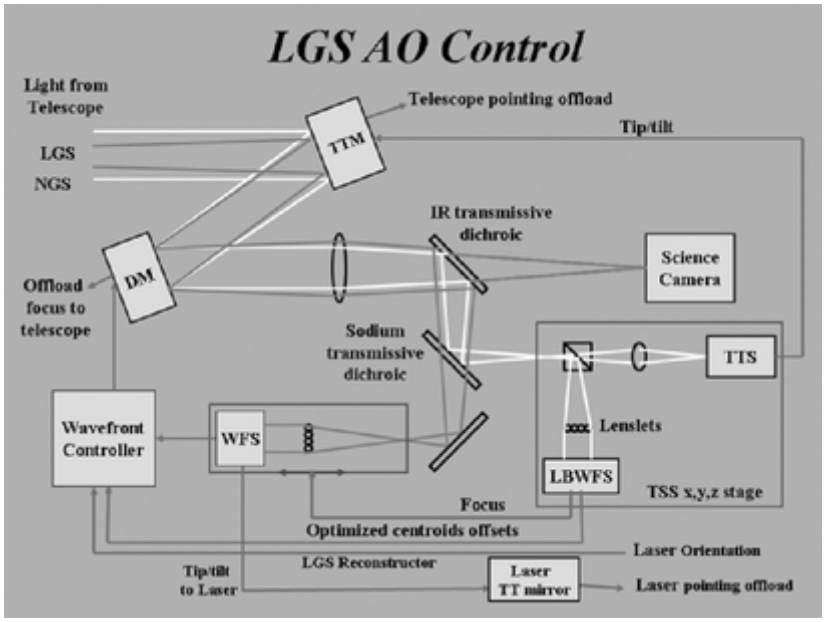

Fig. 1.— Schematic representation of the Keck LGS AO system components. The light from the telescope is reflected off a TTM and DM. The infrared light is transmitted through an IR-transmissive dichroic to the science instrument. The visible light from the NGS and LGS is reflected off this dichroic. The NGS light is reflected off a sodium-transmissive dichroic to a TTS and LBWFS mounted on an (x, y, z) TSS. The transmitted LGS light goes to a WFS mounted on a focus stage. The resulting control loops are described in the text.

The WFS is mounted on a translation stage to keep it conjugate to the sodium layer as a function of zenith angle. The tip-tilt error is used to drive the laser uplink TTM, which in turn offloads to a larger stroke mirror used for laser pointing corrections. The tip-tilt–removed centroid errors measured by the WFS go to the wave-front controller that drives the DM. The DM offloads its time-averaged focus to the telescope control system, which pistons the secondary mirror to compensate.

The visible light reflected off the sodium-transmissive dichroic goes to the tip-tilt sensor (TTS) and low-bandwidth wave-front sensor (LBWFS). A beam-splitter cube transmits 80% of the light to the TTS, since tip-tilt needs to be corrected at a high bandwidth, and reflects 20% to the LBWFS. The TTS and LBWFS are mounted on an (x, y, z)-translation stage (TSS) to acquire and track an off-axis NGS.

The tip-tilt error measured by the TTS is used to drive the TTM, which in turn offloads to the telescope pointing. The focus error measured by the LBWFS is used to keep the WFS conjugate to the sodium layer. The time-averaged centroid errors measured by the LBWFS are used to remove the LGS-induced aberrations by adjusting the WFS centroid offsets. The LGS reconstructor changes as a function of the laser orientation with respect to the WFS.

This last point about laser orientation deserves an explanatory background paragraph, since it is mentioned several times in the next section and is somewhat unique to Keck. In the Keck II case, the laser projects from the elevation ring of the telescope. As the telescope moves in elevation, the laser projector and telescope pupil change in orientation with respect to the fixed Nasmyth platform location of the AO system. In addition, the sky rotates with respect to the AO system as the telescope moves in azimuth and elevation. The first element on the AO bench is a derotator, which can be used to keep either the sky or the pupil fixed with respect to the AO system, but not both. In general, observers prefer to keep the science object orientation fixed on the science instrument, resulting in a changing orientation of the Keck pupil and laser on the WFS. Since the Keck pupil is an irregular hexagonal shape (due to its 36 hexagonal segments), we already had to solve the problem of a rotating pupil for NGS AO (Stomski & Shelton 2000). This is done by continually determining which WFS subapertures are illuminated, and building and loading new reconstructor matrices on this basis. The impact of a rotating off-axis laser projection is among the LGS AO issues addressed in the next section. The NGS and LGS reconstructors are discussed in van Dam et al. (2004) and (2006), respectively.

2.2. LGS AO Issues and Approach

An overview schematic of the LGS AO issues and the solutions we have chosen is shown in Figure 2.

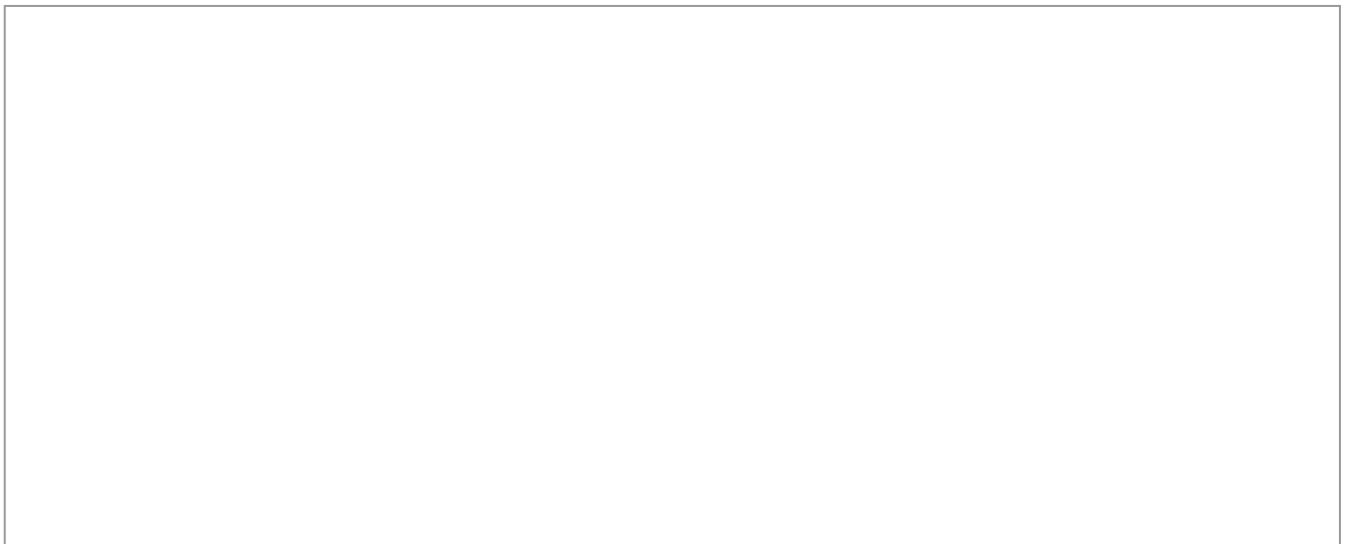

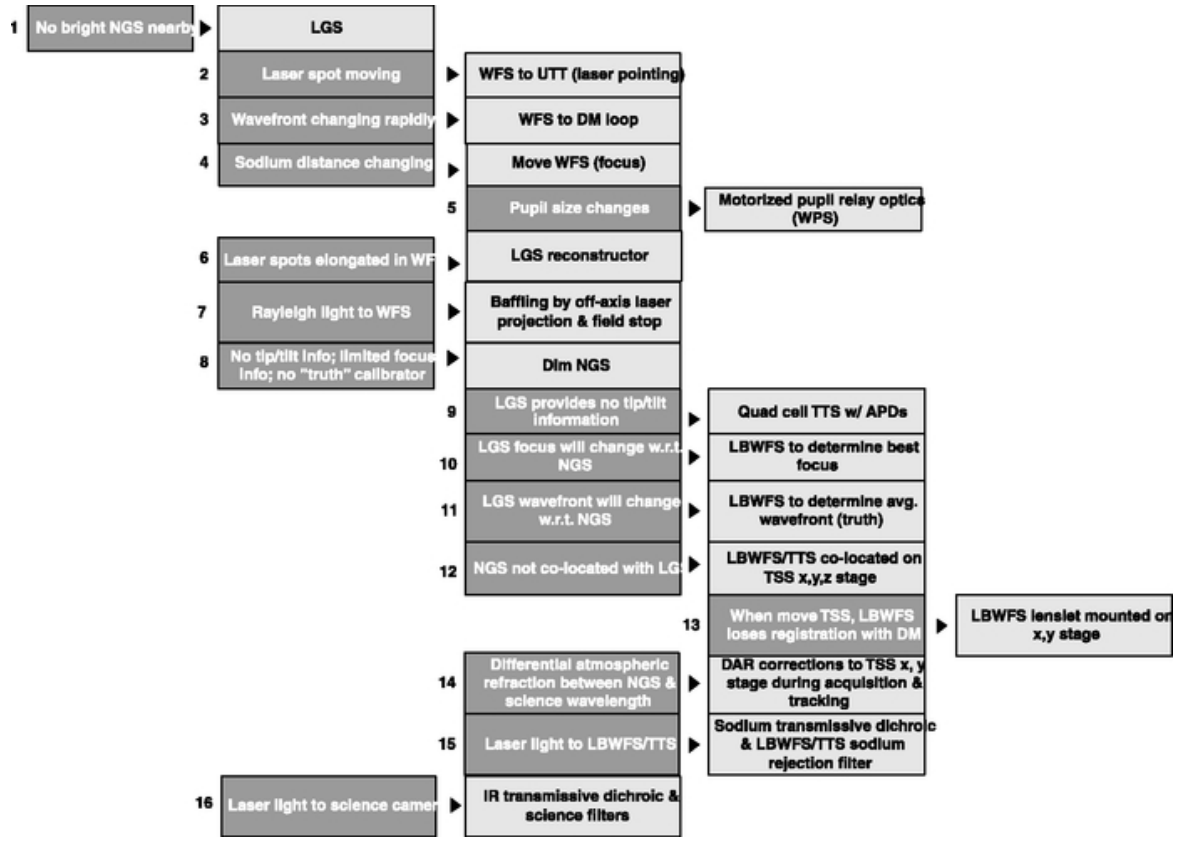

Fig. 2.— Solutions tree for LGS implementation issues. LGS-specific issues are shaded in dark gray below their associated parent topic, and their chosen solution is indicated with an arrow. Individual issues are called out by a number referenced in the text.

In NGS AO, the wave-front distortions introduced by the turbulence in Earth's atmosphere are measured using the light from a star or compact astronomical object. Since the atmosphere changes both temporally and spatially, the NGS must be bright and near the science target. For the Keck NGS AO systems, the NGS must be brighter than 14th magnitude and within 30" of the science target. This limits NGS AO observations to only a small fraction of the sky. The lack of a bright nearby NGS for a hypothetical science target is shown as item 1 in Figure 2. One solution is to use an LGS, specifically a sodium-wavelength LGS in our case.

As shown in Figure 2, there are complications introduced when using an LGS.

Item 2.— The laser spot moves on the sky, due to tilt introduced in the upward path by a combination of atmospheric turbulence, laser launch-tube flexure, telescope vibrations, and wind shake. To overcome this LGS spot motion, the laser launch

optics includes a tip-tilt mirror (referred to as uplink tip-tilt, or UTT) to stabilize laser pointing. The UTT error signal is provided by the WFS, which observes the LGS light. The Keck WFS is a high-bandwidth (up to 670 Hz) Shack-Hartmann system with 20 subapertures across the Keck primary mirror.

Item 3.— Rapid atmospheric turbulence–induced changes in the wave front are corrected by changing the shape of a DM using the tip-tilt–removed wave front measured by this WFS, in the same way as for NGS AO.

Item 4.— In NGS mode, the WFS is located in the same focal plane as the science instrument (i.e., conjugate to infinity), which ensures that the WFS drives the DM to maintain focus on the science instrument. In LGS mode, the WFS needs to be conjugate to the sodium layer so that the LGS is in focus on the WFS. As the telescope moves away from the zenith, the distance to the sodium layer increases, and the WFS focus must be moved back toward the NGS focus to stay conjugate to the sodium layer. The required focus shift as a function of zenith angle ξ is given by

$$Z(h, \xi) = fh/(h - f\cos\xi) - f = (f^2\cos\xi)/(h - f\cos\xi), \quad (1)$$

where h is the height of the sodium layer above the telescope at zenith, and f is the focal length of the telescope (f = 150 m for Keck). For h = 90 km, the Keck WFS focus shift varies from 250 mm at the zenith to 125 mm at a zenith angle of 60°. To avoid having the H-band Strehl ratio degraded by more than 10%, the focus must be maintained to an accuracy of 0.17 mm. The approach taken in the Keck system was to mount the WFS on a focus stage that tracks as a function of the zenith angle.

Item 5.— Translating the WFS in focus also changes the distance to the pupil (i.e., the DM). To compensate, one of the elements of the WFS pupil relay optics is translated. This maintains the pupil size on the WFS lenslet array.

Item 6.— In NGS AO, the reference beacon imaged in each WFS subaperture is identical, regardless of pupil location. In LGS AO, however, each subaperture sees an elongated image of the approximately 10–15 km thick layer of sodium illuminated by the laser. This is due to perspective elongation as one moves off the axis of the laser projection telescope. The elongation is a function of the distance off the laser projector axis and is in the direction of the laser projector. This is particularly bad in the Keck II laser implementation, since the laser projector is located on the side of the telescope. The subaperture on the far side of the telescope from the projector (~12 m from the projector) exhibits an elongation as long as 3" for a 10 km thick layer at an altitude of 90 km. Figure 3 (*middle*) shows an acquisition camera image of this LGS elongation versus distance obtained by unstacking the 36 primary-mirror segments of the Keck Telescope; the bright spot on the right side of this image is the Rayleigh-scattered light from air molecules in the lower atmosphere, indicating the side where the laser projector is located. This elongation introduces several challenges. One is that the optimal (x, y) gains for each subaperture are functions of the length and direction of the elongation, and the other is that these gains change as the pupil (and hence laser projector) rotates. This gain versus position correction is handled in the LGS wave-front reconstructor, and the reconstructor is updated as the telescope pupil rotates with respect to the AO system. The LGS reconstructor algorithm takes two inputs to estimate spot size in each subaperture: the FWHM of the laser spot as seen from near the launch telescope, and the maximum elongation observed at the far edge of the pupil. Both of these are measured nightly from acquisition camera images of the unstacked primary-mirror segments. Projecting the laser from behind the secondary mirror instead of from the side of the telescope would have considerably reduced the complexity of this issue (and item 11 below), since the magnitude of the elongation would be halved and the impact of pupil rotation could be negligible.

Item 7.— The Rayleigh-scattered light could contaminate the measurements made by the WFS if it reached this sensor. The Rayleigh light is separated from the LGS light due to the off-axis projection of the laser, and this off-axis Rayleigh light is then blocked by the field stop in front of the WFS.

Item 8.— Some critical information cannot be obtained from the LGS. This information can be provided by a faint NGS.

Item 9.— Unfortunately, the LGS does not provide tip-tilt information for the science object, since the laser is deflected in tip and tilt along both its upward and downward paths. A separate TTS observing an NGS can be used to provide this tip-tilt information. NGSs as faint as 19th magnitude can be used with the Keck system's TTS. The error measured by this sensor is used to drive a fast TTM.

Item 10.— A change in the altitude of the sodium layer looks like a focus change to the WFS and is therefore applied to the DM. An LBWFS aimed at the NGS that is being used for tip-tilt is employed to sense this error. The WFS focus stage position is adjusted to drive the time-averaged focus measured by the LBWFS to zero. The new focus-stage position is then used to reestimate the sodium layer altitude to optimize the focus-stage tracking rate (Summers et al. 2004).

Item 11.— The wave front measured by the WFS is different when an LGS is used than when an NGS is used. In particular, the LGS elongation mentioned under item 6 above results in the measurement of aberrations that one does not want to apply to the DM. These are referred to as semistatic, since they change as the sodium layer thickness or structure changes, as the telescope elevation changes, and as the telescope pupil (and hence laser projector) rotates. In the case of Keck, a LBWFS is used as a truth sensor to correct for these aberrations. The LBWFS determines what centroid offsets should optimally be applied to each subaperture of the fast WFS observing the LGS. The bandwidth of the LBWFS is limited by the magnitude of the available NGS to an exposure time of tens of seconds to a couple of minutes. A model of the LGS aberrations can be used to provide higher bandwidth corrections when the NGS is too faint or when the pupil is rotating more rapidly than can be compensated for by the LBWFS.

Item 12.— The LGS is normally pointed at the science object somewhere in the field of view of the science camera. The NGS can be separated from the science object by as much as about 60", due to the large isokinetic angle for tip-tilt correction. In the Keck system, the TTS and LBWFS are located on a three-axis TSS to allow off-axis acquisition of this NGS. Focus tracking versus field position is automatically provided by one of these axes to compensate for the curvature of

the focal plane. This axis also provides focus adjustment to match the focal position for different science instruments.

Item 13.— Translation of the LBWFS around the field to acquire the NGS results in a misregistration of the LBWFS's lenslets with respect to the DM (by as much as 0.58 subapertures at the edge of the field). The lenslets are mounted on an (x, y)-translation stage to maintain registration with the DM actuators.

Item 14.— Acquisition and tracking of the NGS on the LBWFS and TTS includes compensation for differential atmospheric refraction (DAR) between the wavelength observed by the science instrument and the tip-tilt sensor, in order to accurately acquire and maintain the science object's position on the science instrument. DAR compensation is a function of the telescope's elevation, the color of the NGS, and the wavelength of the science observation (Stomski et al. 2003).

Item 15.— Due to the faintness of the NGS, the complete rejection of the sodium light becomes crucial. A sodium-transmissive, visible-reflecting dichroic beam splitter is used to reflect the NGS light to the TTS and LBWFS (the transmitted light goes to the WFS). This provides partial rejection. In addition, a narrowband rejection filter (centered on the 589.3 nm laser line) is located in front of the TTS and LBWFS

Item 16.— In the case of infrared science instruments, the sodium light can be rejected through the use of an IR-transmissive dichroic and the science instrument filters and detectors.

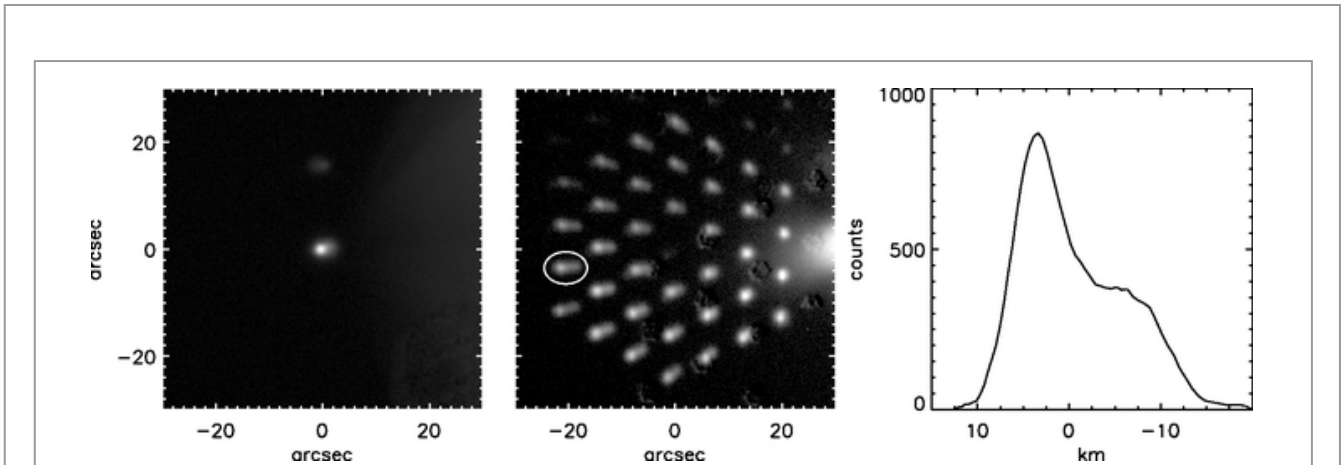

Fig. 3.— Acquisition camera images (*left and middle*; 60″ × 60″) of the Keck LGS at zenith. *Left*: LGS image with a FWHM of 1.″6 × 2.″0 and an equivalent *V* magnitude of 9.8. *Middle*: LGS image taken with the 36 primary-mirror segments unstacked. The laser projector is on the right side of the telescope in these images; the side from which the Rayleigh-scattered light can also be seen. The individual segment image closest to the projector can have a FWHM as small as 1.″0, while the segment images further away can be seen to be elongated toward the projector. The circled segment image in the middle panel was used to produce the relative density structure vs. altitude plot for the sodium layer (*right*); a 35 km altitude range is shown.

2.3. Optomechanical Implementation

The NGS AO facilities are located on the left Nasmyth platforms of the Keck Telescopes at the f/15 focus. The entire facility is enclosed in the thermally insulated enclosure shown in Figure 4, with one room for the AO bench and science instruments, and a second room for the electronics racks.

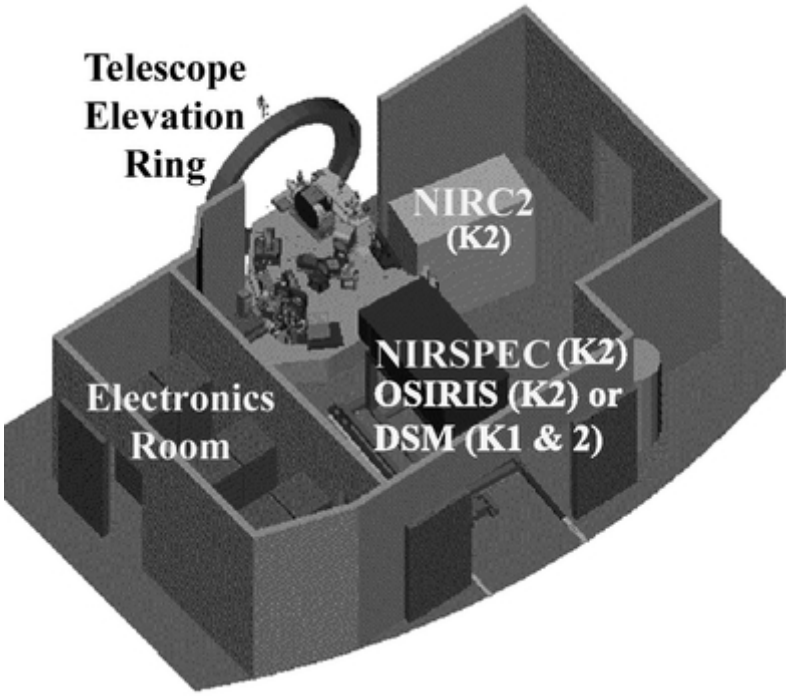

Fig. 4.— Schematic view of the Keck AO enclosure, located on the left Nasmyth platform of the telescope, with its roof removed. Light from the telescope enters the AO bench through the telescope elevation ring.

Science instruments can be positioned at two locations next to the AO bench as shown in Figure 4. NIRC2 is located at a fixed position, while NIRSPEC, OSIRIS, and the dual star module (DSM), which feeds the interferometer in the basement between the two Keck Telescopes, move in on rails to kinematic defining points located beside the AO bench.

Figure 5 provides a top-view schematic of the AO bench. The light from the telescope comes to a focus just inside the derotator (labeled 1 on Fig. 5). The derotator, which consists of three flat mirrors, can be used to keep either the image or the pupil fixed. The next element (2) is a fast tip-tilt mirror consisting of a 203 mm diameter silicon carbide mirror with three piezoelectric actuators. The beam continues to diverge to an off-axis parabola (3) that collimates the light and reimages the primary mirror of the telescope onto the DM (4). The Xinetics, Inc., DM has 349 electrostrictive actuators on a 7 mm spacing, corresponding to 56 cm spacing on the primary mirror. The second off-axis parabola (6) reconverges the light with the same focal ratio and exit pupil location as initially provided by the telescope. The light is split at a visible-reflecting, IR-transmitting dichroic (7). The infrared light (>1 μm wavelength) proceeds either directly to NIRC2 or off a fold mirror (9) to OSIRIS, or off another fold mirror (10) to NIRSPEC. Since NIRSPEC was designed as a seeing-limited instrument, a set of reflective reimaging optics (30–34) was implemented to provide a factor of 10 magnification to take advantage of the increased angular resolution behind AO while maintaining the pupil and image position within NIRSPEC. The light to the DSM that feeds the interferometer is picked off in collimated space by an IR-reflective, visible-transmitting dichroic (5).

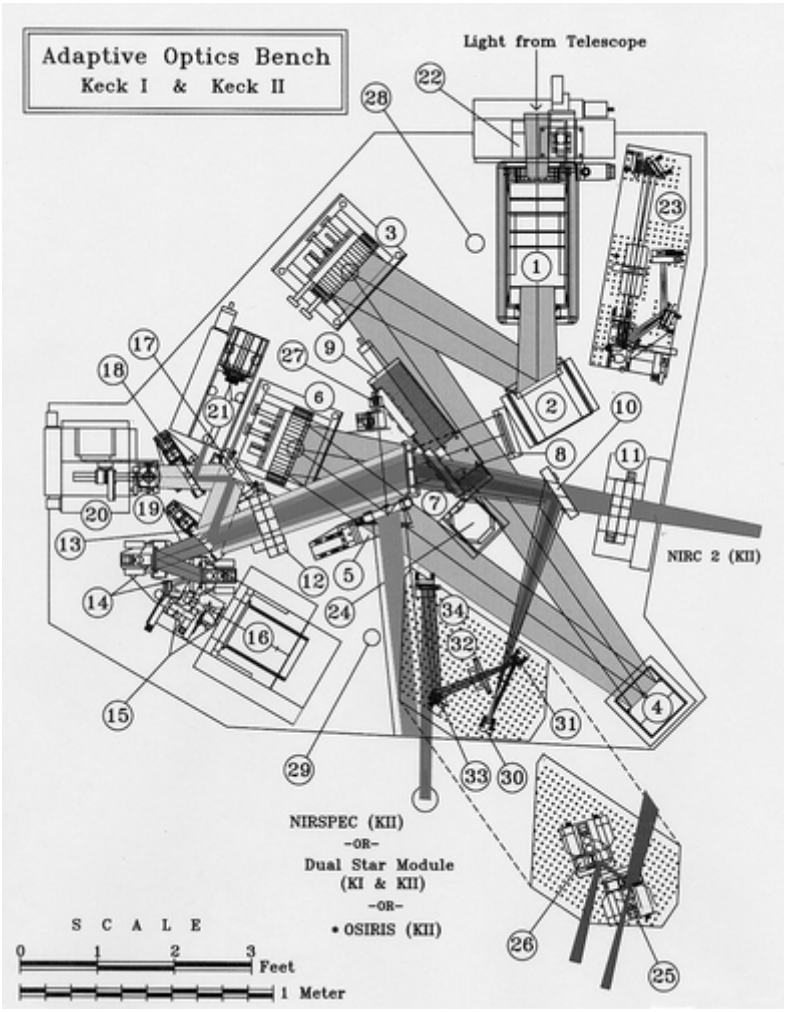

Fig. 5.— Schematic aerial view of the AO optics bench. The numbers are referenced in the text.

The visible-reflecting dichroic (7) sends the visible light toward the various wave-front sensors. A translation stage (13) allows the selection of either a 4% reflective beam splitter for NGS mode or a visible-reflecting, sodium-transmitting dichroic for LGS mode. The transmitted light proceeds to a pair of field-steering mirrors (14), which select an object within the available field of view (up to 40″ off-axis) and direct it down the axis of the Shack-Hartman wave-front sensor optics (15) and camera (16). These optics consist of a field stop, transmissive optics that reimage the DM onto an array of 200 μm square lenslets, and transmissive optics that relay and demagnify the images from the lenslets onto the Adaptive Optics Associates camera. The MIT/LL CCD consists of 64 × 64, 21 μm square pixels. The image from each lenslet is reimaged onto 2 × 2 pixels, with 1 pixel between subapertures. The entire WFS assembly, from the field stop to the camera, is mounted on a translation stage to maintain conjugation to the sodium layer.

A translation stage (18) allows a mirror to be inserted to feed the light toward the 2′ diameter field of view of the acquisition camera (21). In LGS mode, this mirror is translated out of the beam, and the NGS light is sent to the LBWFS (19) and the TTS (20), mounted on an (*x*, *y*, *z*)-translation stage, as shown in Figure 6. STRAP is a quadrant avalanche photodiode unit manufactured by Microgate. The light to STRAP is collimated through a filter wheel and then reimaged at a slower focal ratio (f/37.5) onto the quad lenslet of STRAP. After reflection off an 80:20 beam splitter, light heading toward the LBWFS goes through a lens and field stop mounted in a lens-tube assembly. The light is then collimated before passing through a lenslet array mounted on an (*x*, *y*) motorized stage. The lenslets are imaged on a Photometrics 512 × 512 CCD detector. The LBWFS lenslets are registered to the DM actuators in a pattern identical to the WFS lenslets, but with 16 × 16 pixels per subaperture instead of 2 × 2 pixels.

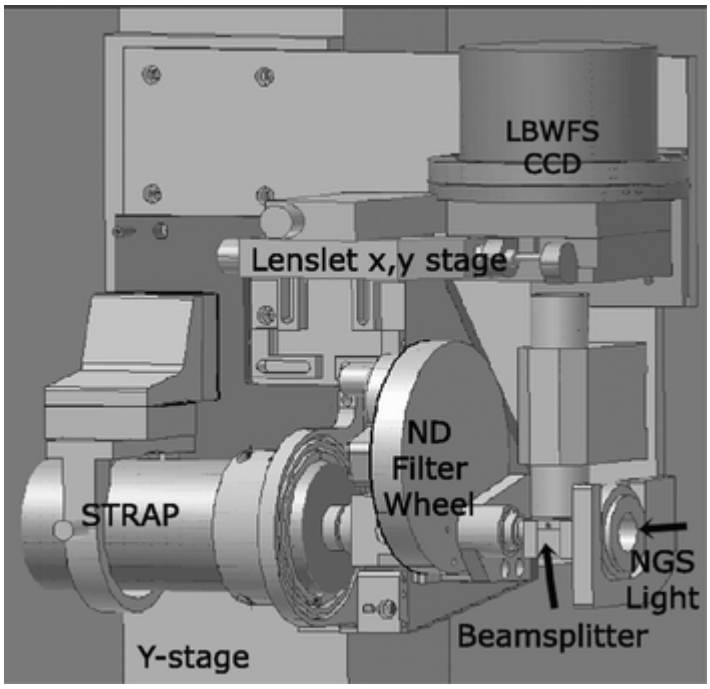

Fig. 6.— CAD drawing of the STRAP tip-tilt sensor and LBWFS.

3. LASER GUIDE STAR

3.1. Laser System

A schematic of the laser system location is shown in Figure 7. A thermally insulated laser room on the dome floor houses six flash-lamp–pumped, frequency-doubled Nd-YAG lasers and a dye master oscillator (DMO), plus associated hardware and safety systems. The DMO is narrowly tuned to the center of the sodium doublet wavelength. The DMO's output is broadened across the doublet with a pair of electro-optic phase modulators and then coupled into a single-mode fiber. The single-mode fiber provides the seed light to a table on the side of the telescope, where it passes through two stages of dye amplification (preamplifier and amplifier stages). The YAG lasers, coupled through multimode fibers, are used to pump the various dye laser and amplification stages. These lasers are *Q*-switched at either 13 or 26 kHz, with pulse durations of 150 ns, and each produces about 40 W of output power. The 26 kHz versions are used to pump the DMO and preamplifier. The four 13 kHz versions, two of which are time delayed to produce an overall 26 kHz pulse rate, are used to pump the amplifier.

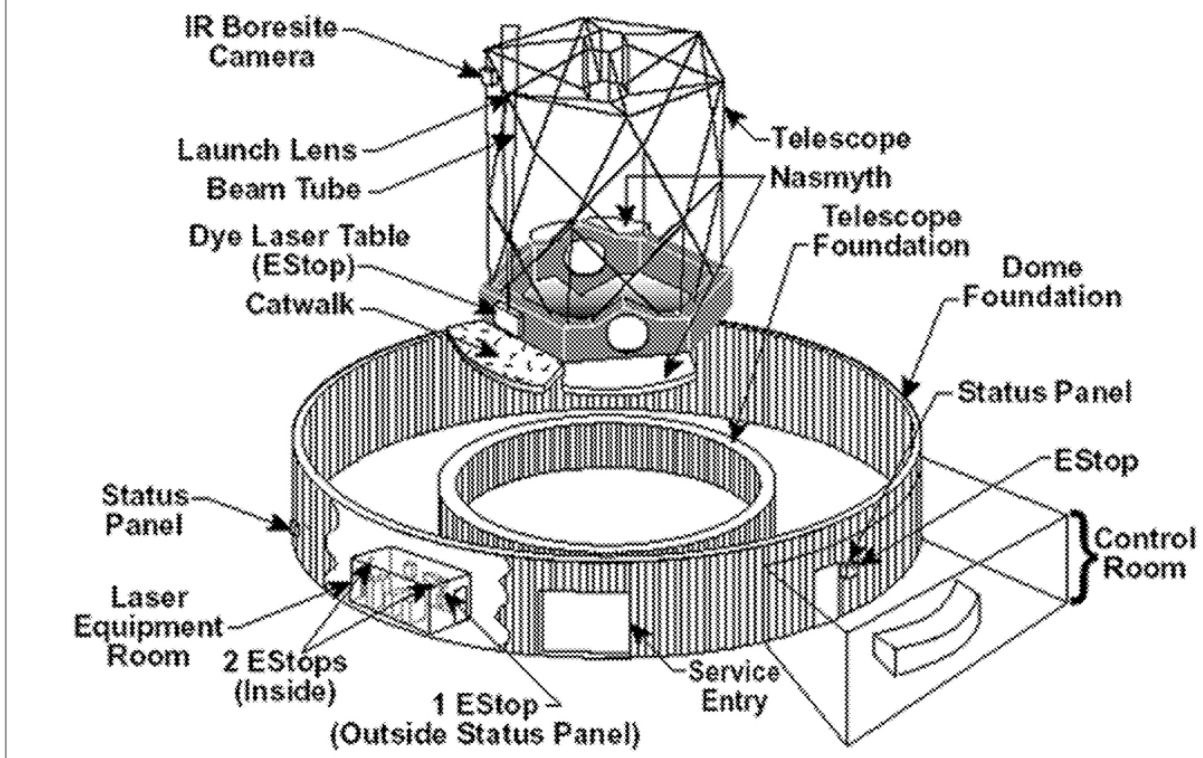

Fig. 7.— Schematic of the location of the laser equipment room on the dome floor, the dye laser table, and the projection telescope (beam tube and launch lens), and the IR boresight camera on the side of the telescope.

A 1.2 × 1.8 m laser table, shown in Figure 8, is located vertically in an enclosure on the elevation ring of the telescope. In addition to the two stages of dye amplifiers, a significant number of transport and formatting optics, and the first element of the projection telescope, this table contains several alignment and diagnostic tools. These tools include power meters, a power-in-the-bucket camera, and pointing and centering cameras. The last element on the laser table is a pointing mirror that is used to center the laser with respect to the science object and to compensate for tilt changes due to flexure and the distance to the sodium layer (Summers et al. 2004).

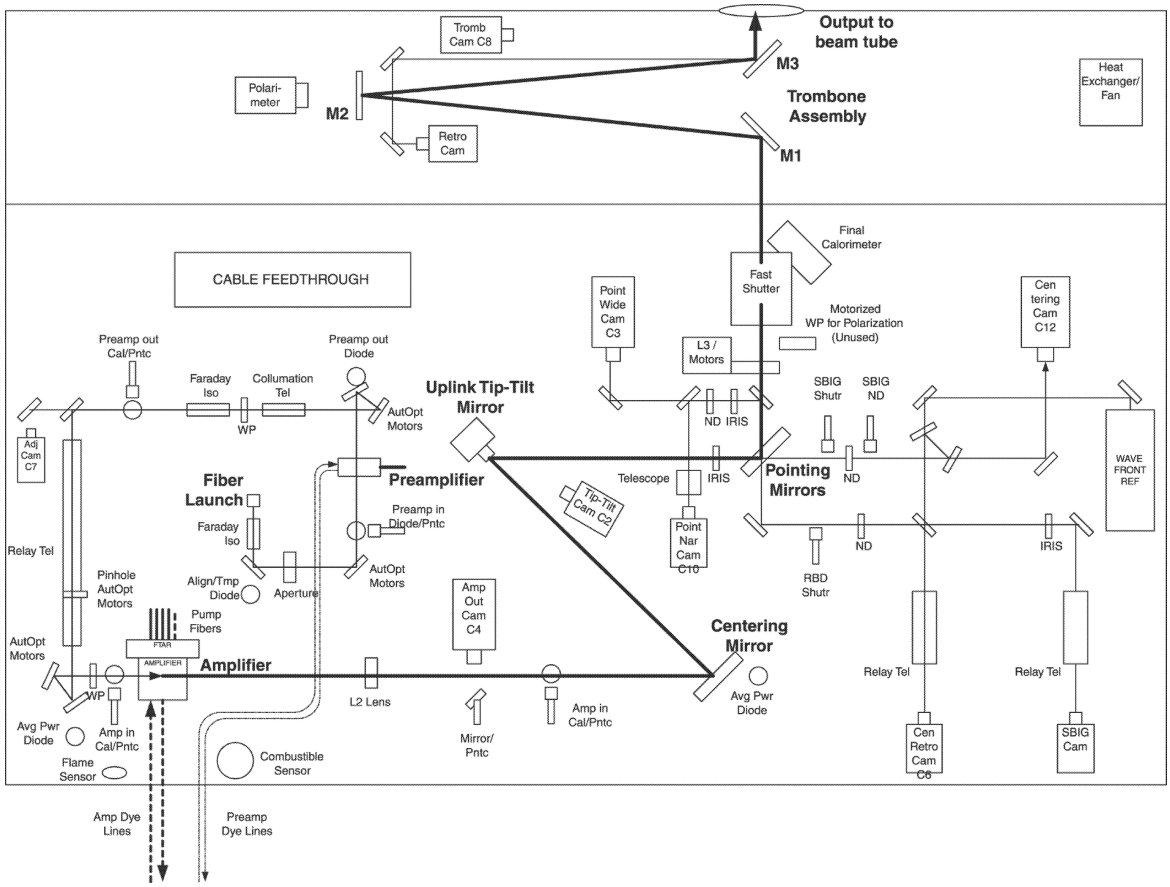

Fig. 8.— Schematic view of the 1.2 × 1.8 m laser table and the trombone assembly mounted on the elevation ring of the telescope. The dark solid line shows the optical path from the laser amplifier cell off of the centering mirror, UTT mirror, and pointing mirror, through a three-mirror trombone assembly to the output up the beam tube. A portion of the light is split off at or near the pointing mirror to several diagnostics cameras. The light path prior to the amplifier begins at the fiber launch (a single-mode fiber from the dye master oscillator on the dome floor) and passes through the preamplifier and various formatting optics.

The final output of the dye laser is sent to the sky through a projection telescope with a 50 cm diameter output lens, mounted to the side of the telescope. Both the laser table and the projection telescope move with the telescope in azimuth and elevation. An extensive programmable logic control safety system is in place to protect personnel and the laser itself.

The major weak point of the current laser system is its overall complexity (nine lasers in total). Failure points include the YAGs, especially the use of flash lamps, and the inherent difficulties of dye lasers, including many dye-cell burns in our early days. The wall-plug efficiency is also low, with ~50 kW producing ~12 W of output power. Sodium-wavelength solid-state lasers, which were unavailable when we started this project, are much less complex and should be far more efficient and reliable.

3.2. Laser Operation and Coordination

Safety systems are in place to protect aircraft and satellites. Our Federal Aviation Administration–approved approach to aircraft safety is to have two spotters outside during all laser operations, with switches to shutter the laser. We also have an IR camera boresighted to the laser that will automatically shutter the laser in the event of aircraft detection. Given Hawaii's location in the middle of the Pacific, we have only had to shutter the laser for an aircraft a couple of times. Our longer term plans include the implementation of a visible wide-field camera system for aircraft detection, and possibly the use of a Hawaii-wide radar feed to alleviate the need for spotters.

Prior to each laser observing run, a list of targets and their observation times is faxed to the Laser Clearinghouse at the US Space Control Center. The Space Control Center faxes back a list of any required blackout periods, to avoid illuminating satellites. This has had minimal impact on our nighttime operations to date, since blackout periods have been rare, but it requires careful preobserving planning.

A laser traffic control system (LTCS) is also in place to ensure that the laser does not contaminate the observations of other telescopes (Summers et al. 2003). All the potentially affected telescopes on Mauna Kea provide their current pointing coordinates to the LTCS via a URL, along with additional parameters such as field of view, and the laser is automatically shuttered by the LTCS when the laser passes through their field of view. The surface brightness of the Keck laser measured by the Subaru Telescope at elevation angles between

45° and 60° was found to be relatively low, roughly equivalent to 19.5 mag arcsec^{-2}; however, the impact could be significant if the intersection were to occur near the LGS itself (Hayano et al. 2003).

See Wizinowich et al. (1998) for a discussion of the coordination and use of laser beacons on Mauna Kea.

3.3. Laser Guide Star

The performance of the LGS AO system depends on the power and beam quality of the laser and the density and structure of the sodium layer. The laser is typically operated at an output power of between 12 and 14 W. Depending on the sodium density, this generates an LGS with an equivalent *V* magnitude of typically 9.5 to 10.5 mag at the zenith (or ~140 to 55 photons s^{-1} cm^{-2}). The return decreases with zenith angle, due to the resulting increase in the distance to the sodium layer and the amount of Rayleigh scatter.

The FWHM of the LGS image as seen by the subapertures closest to the laser launch telescope is typically 1.″0 to 1.″4. As seen in Figure 3, the images appear elongated as the subapertures become farther away from the launch telescope. This elongation has been observed to be 3.″4 FWHM for a sodium layer thickness of approximately 15 km. A fairly commonly observed structure for the sodium layer versus altitude can also be seen in the right panel of Figure 3.

4. OBSERVING OPERATIONS

4.1. NGS Operations

During NGS science operations, the astronomer operates the science instrument from the remote operations room at Keck Observatory's headquarters, and the observing assistant (OA) operates the AO system from the telescope control room on Mauna Kea. The daytime AO calibrations take less than 30 minutes and include calibrating the DM-to-lenslet registration and the non–common-path aberrations between the science instrument and the WFS optical paths. These are performed by a support astronomer using a set of calibration tools. A more thorough set of AO calibrations (WFS lenslet centering, telescope pointing origins, and image sharpening on the science instrument) is performed by an AO expert prior to the first night of an observing run.

At dusk, the OA brings up the AO observing tools and runs a script that automatically configures the AO system for the specific science instrument and telescope (Keck I or II). The OA also acquires each new target before turning over control to the astronomer. The automated tools perform the AO acquisition using the *V* and B - V magnitudes for the NGS provided by the astronomer's star list. The DAR-compensation tool positions the science object at the desired location on the science instrument by compensating for DAR with the field-steering mirrors (FSMs) that feed the WFS. The autosetting tool commands the AO subsystems and the telescope to obtain sky backgrounds and set the WFS frame rate, the tip-tilt and DM gains, and if necessary (for bright objects), the camera gain and WFS neutral density filters; it iterates once, if appropriate, using the photon flux measured by the WFS to find the optimal settings. The OA monitors the status and health of the AO system with dedicated tools that also automatically recover from faults. After slewing to a new target, AO acquisition takes between 30 and 90 s, depending on the object brightness and the sky transparency conditions.

Once the AO acquisition is complete, the astronomer selects the science instrument configuration, including the rotator mode and position angle, and then controls the observing sequence using the science instrument user interfaces. Many possible dithering scripts that are common to near-infrared imaging and spectroscopic observations are commanded from the science instrument user interface. A handshake protocol is used to automatically coordinate the telescope and AO system during these dithers. This includes opening the AO loops, repointing the telescope and FSMs, and closing the AO loops.

The main observing-time overheads in NGS AO observing are telescope slew, telescope fine-acquisition on target (<2 minutes), AO acquisition (90 s), and AO/telescope/instrument handshaking during dither (8–10 s per dither command). When using NIRC2, the NIRC2 setup (20 s for filter/camera moves) and readout (~8 s frame^{-1}) times also impact observing efficiency. Some specific observing modes, such as coronagraphy and spectroscopy, require more setup time to center the target with a 10 mas accuracy behind the focal mask or on the spectroscopic slit. The observing efficiency throughout an AO night ranges from 60% (1–2.5 μm wavelength deep AO imaging) to 30% (survey-mode observing, or 3–5 μm observing that requires lots of frames and dither).

4.2. LGS Operations

LGS AO observing preparations currently start a week prior to an observing run, with a meeting between the support astronomer and the observers. A Web page has been set up to support observation planning.[4] This includes a description of the system and the observing procedures. Also available are software tools for finding suitable NGSs, supporting the generation of star lists, and planning for off-axis observations. All science targets are reviewed for technical feasibility with the support astronomer. Prior to observing, the astronomer also becomes acquainted with the science camera and the specific LGS dithering scripts.

Supporting LGS AO represents a significant load on the Observatory. The minimal LGS-specific operation crew for an observing night includes a laser technician to start up the laser in the afternoon and monitor the laser and LTCS during the early evening, a second laser technician to monitor these systems through the remainder of the night, an LGS AO operator, a support astronomer to monitor and optimize the LGS AO system, and a team of aircraft spotters. This is in addition to an OA who operates the telescope, and a support astronomer for the science instrument. Ultimately, we plan to reduce the LGS-specific operations crew to an afternoon laser technician and a nighttime LGS AO operator. This will be done by implementing automated systems for aircraft detection and laser system monitoring, transferring some responsibilities to the OA, and training the LGS AO operator in system optimization.

Prior to an observing run, about 2 hr of afternoon NGS and LGS AO calibrations and system checkout are performed on the system. Daily start-up and checks of the laser system by a technician take 2 to 3 hr, with a full day of alignments and checks on the first day of the run. The laser also requires considerable routine maintenance and recovery from component failures.

An LGS operator is currently required to operate the LGS system for observing. The long-term plan is to have the OA operate the LGS AO system, as is done for NGS AO observing. So far, one OA has been trained as an LGS AO operator.

Beginning at dusk, a 40 minute routine test procedure is performed to check out the AO system in NGS mode, measure the seeing, acquire and characterize the LGS at zenith, and check out and characterize the AO system in LGS mode on a fairly bright star (*R*-band magnitude of ~10). Laser propagation is restricted to between 12° twilight after sunset and before dawn.

Acquisition of a new target in LGS AO mode is somewhat complex, due to the requirement that two properties of the sodium layer must be determined before science integrations can begin. One is the altitude of the layer, and the other is the effect of the layer's structure and thickness on the wave front measured by the WFS. Both of these are determined iteratively by observing the wave front of an NGS with the LBWFS while locked on the LGS with the WFS.

The following is a typical LGS AO acquisition sequence: the OA slews to the science target as instructed by the observer and positions the tip-tilt reference NGS on the acquisition camera at a location that coincides with the desired position on the science camera. Using the color information of the star, DAR correction is automatically used to position the STRAP/LBWFS stage for NGS acquisition.

The LGS operator then takes over and, similarly to NGS AO acquisition, uses fully automated scripts to set the subsystem parameters, interact with the telescope for recording background for the various sensors, and acquire the NGS and offset to the science target. The *R*-band magnitude of the NGS is used to set up the LBWFS binning and integration time and the TTS gain and integration time. The tip-tilt loop is closed on the NGS. The laser is projected toward the NGS, and the DM loop is closed on the LGS. LBWFS measurements are then begun on the NGS. The LBWFS measurements are used to (1) optimize the WFS centroids (to correct for the varying extension of the LGS spot across the telescope pupil) and (2) focus the WFS (to be conjugate to the sodium altitude). Since LBWFS integrations are necessarily very long (~120 s) when using a faint NGS ($R > 18$ mag), the initial determination of these properties may be more efficiently done on a nearby bright star prior to acquisition of the science target's NGS. Each LBWFS wave-front measurement is used to iteratively converge on the correct WFS centroid offsets and focus until the measured rms wave-front error has fallen below 200 nm (usually three to five LBWFS integrations). The LGS AO performance is optimized and monitored during the observations. The tip-tilt and DM loop gains and bandwidths can be manually adjusted using an optimization tool that analyzes saved WFS and STRAP telemetry data. If appropriate, the telescope is then offset to the science target. This automatically opens the tip-tilt and LBWFS loops, repoints the telescope and the TTS/LBWFS stage, and recloses these two loops.

The entire acquisition takes 5 minutes for stars brighter than 16 mag, and up to 15 minutes for faint stars (19 mag) or objects that require manual tuning during acquisition (e.g., extended targets with high-intensity backgrounds, such as M31).

Control is then handed back to the astronomer to begin science observations. At the start of an observing sequence, typically both the LGS and the science target are positioned at the center of the science camera. During dithering scripts, the astronomer has the option of leaving the LGS fixed at the center of the science camera field or on top of the science object when the science object is repositioned on the science instrument. In the latter case, if the DM loop is initially closed, then repointing the telescope will automatically open the DM and uplink tip-tilt loops, reposition the laser pointing mirror and the WFS FSMs, and reclose the loops. If the TTS loop is closed, then repointing the telescope will always open the TTS and LBWFS loops, reposition the STRAP/LBWFS stage to reacquire the NGS with DAR corrections, and reclose these loops.

5. THE SCIENCE FACILITY

5.1. NGS Science Capability

The performance of the Keck II NGS AO system is reported in van Dam et al. (2004). The achieved on-axis *H*-band Strehl ratio varies from 0.4 for stars brighter than V = 9 to 0.1 for V = 14. NGSs can be used as far off-axis as 40".

Keck NGS AO science output has included the publication of 74 refereed science papers as of 2005 October, including seven papers with the interferometer. Keck Observatory staff maintain a bibliography of refereed Keck AO science papers.[5] The mix of these papers is 31% planetary, 54% Galactic, and 15% extragalactic. Solar system science has included observations of planets, especially Neptune and Uranus, moons of planets such as Io and Titan, and asteroids. One feature that has made the Keck II system especially suitable for planetary science is that the WFS can close on objects as large as 4" in diameter. Galactic science has included companion searches and orbits, circumstellar disks, pre–planetary nebulae, and astrometric and spectroscopic measurements of the stars orbiting the black hole at the center of our Galaxy. Extragalactic science has been limited to faint galaxies near bright stars and galaxies with bright cores, a limitation that has been dramatically reduced with LGS AO.

5.2. LGS Science

5.2.1. Science Demonstration Program

An LGS engineering science program was implemented to test and demonstrate the most challenging observing modes in a realistic way, and to provide an opportunity for early scientific use of the system. Projects spanning planetary, Galactic, and extragalactic astronomy were proposed by members of the Keck user community, and the observations were performed by the Keck AO engineering team during commissioning nights.

Initial engineering science projects included observations of the HK Tau binary disk system during our first closed-loop demonstration in 2003 September, and observations of the Egg pre–planetary nebula in 2004 June (Bouchez et al. 2004). The angular resolutions of the Egg Nebula images are 3 to 4 times higher than that achieved with NICMOS on the *Hubble Space Telescope*.

The Galactic center was observed for 1.5 hr in K' and L' in 2004 July for the primary purpose of comparing LGS AO performance to previous NGS AO data (Ghez et al. 2005). The improvement in performance was dramatic, as shown in Figure 9. In addition, an $80'' \times 80''$ wide-field mosaic in He I and H_2 (1–0) of the region surrounding the Galactic center was also acquired on the same night, in a total observing time of 0.3 hr. These images have provided an excellent demonstration of the wide-field capabilities of the LGS AO system. Since the laser can remain at the center of each element of the mosaic, and the isokinetic angle for the tip-tilt star is large, the image quality remains essentially constant over the entire field.

Observations of the CATS (Center for Adaptive Optics Treasury Survey) fields were proposed to compare LGS and NGS performance on faint extragalactic targets, and to target particularly interesting galaxies (*Chandra* sources and high-redshift candidates) in previously inaccessible CATS fields. A field near guide star GOODS-S19 was observed for 3 hr in 2004 October. The resulting images of merging galaxies have been published in Melbourne et al. (2005).

Solar system engineering science projects have included measuring the system mass of binary Trojan asteroids (Marchis et al. 2005) and Kuiper Belt objects (Brown et al. 2005). Additional projects have included a search for brown dwarf binaries, and images of the Andromeda galaxy shown in Figure 10.

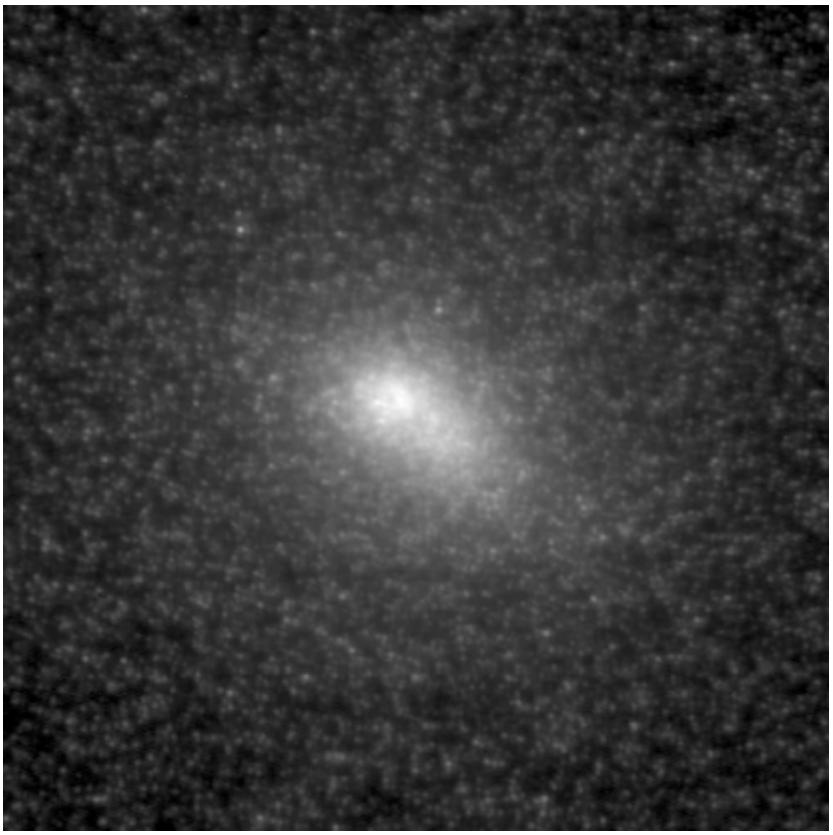

Fig. 10.— A 10″ × 10″ image of the core of the Andromeda galaxy imaged at K' (2.1 μm). A compact cluster 55″ away was used as the tip-tilt reference. The dynamical center of the galaxy, the likely location of a supermassive black hole, is located ~1″ to the lower right of the highest density region. Individual giant stars are clearly resolved throughout the image.

5.2.2. Shared-Risk Science Programs

A restricted number of LGS AO shared-risk science nights with NIRC2 (12) were awarded by the Keck time allocation committees in semester 2005A (February–August), while development continued on the LGS system. As of 2005 October, six refereed papers had been accepted for publication (Gal-Yam et al. 2005; Liu et al. 2005; see also papers cited in § 5.2.1).

5.3. LGS Science Observing Efficiency

The observing time overheads associated with LGS AO are summarized in Table 1. The AO/telescope/instrument handshake during dithers takes 7 s when the LGS is fixed with respect to the center of the science camera, and 20 s when the LGS is moved in order to be

fixed with respect to the science target. NIRC2 overheads remain the same. The average science integration time for two science nights in 2005 March, with three different observers, was 44% of the observing hours.

TABLE 1
LGS AO Observing Overheads

Action	Time
AO setup and laser acquisition (from 12° twilight)	30 minutes
Acquisition of new target (TT ref. $R < 15.5$)	5 minutes
Acquisition of new target (TT ref. $15.5 < R < 19.0$)	10 minutes
Dither with laser move	20 s
Dither without laser move	7 s
Recovery from aircraft or LTCS shuttering of the laser	2 minutes

Note.—These numbers reflect performance as of 2005 July.

The percentage of clear time lost to LGS AO system faults over 12 science nights in 2005 March through July was 12% overall. The time lost was <5% on half of these nights. On two nights, problems with the laser and laser pointing systems, respectively, which are counted as time lost to LGS AO, did not permit laser propagation. On these two nights, we switched to backup NGS AO science programs for half the night.

The average time lost to LTCS collisions during these 12 nights was 17 minutes. We are working with other observatories to minimize the number of these collisions by better understanding the actual impact on their observations. In addition, the Space Control Center has occasionally (once per ~15 nights) required that the laser not be propagated for up to 2 hr, due to a space event, such as a satellite launch.

5.4. Keck LGS Science Capability

The performance of the Keck II LGS AO system is reported in van Dam et al. (2006). The typical achieved on-axis K'-band Strehl ratio varies from 0.35 for NGS stars brighter than R = 10, to 0.27 for R = 16, to 0.1 for R = 19. The performance characterization is an ongoing project that is being documented on the Keck Observatory Laser Guide Star Adaptive Optics observation support Web page (see footnote 3).

During semester 2004B, we demonstrated the following observing modes:

1. Science target <70″ from the tip-tilt (NGS) reference (pupil angle restrictions occur for >55″).

2. NGS reference R<19 in vertical angle (fixed pupil) mode (requires on-axis NGS).

3. NGS reference R<18 in position angle (fixed field) mode, if pupil rotation <2° minute^{-1}.

4. Dithering over up to a 40″ × 40″ square (no faster than every 2 minutes).

5. Observations that require <20 mas positioning accuracy on the science instrument.

6. Observations that require differential atmospheric refraction tracking of the science target (e.g., spectroscopy).

Our user community has been very enthusiastic about the science capability of LGS AO, and increased availability has been strongly encouraged. The number of LGS AO science nights continues to be restricted in semester 2005B (August–January); however, the number of scheduled science nights has been significantly increased to 30, including eight nights with the newly commissioned OSIRIS science instrument. LGS AO development will be quite limited during 2005B to better focus on LGS AO operations, including improved observing automation, better management and maintenance of the laser and AO systems, more training for the observing support group, and completion of the LGS AO performance characterization effort.

6. CONCLUSION

We have described the approach taken in the implementation of a laser guide star system on the Keck II system, as well as the early scientific capabilities. An impressive amount of science has already been achieved with the AO facilities described in this paper, and the future for high angular resolution astronomy at the W. M. Keck Observatory looks extremely promising.

This future includes further improvements to the Keck II LGS AO system, upgrades to the real-time wave-front processor system and wave-front sensor cameras, the implementation of a commercial solid-state laser on the Keck I Telescope, along with laser projection from behind the secondary mirror, and potentially a next-generation LGS AO system.

Financial support for the development and fabrication of the Keck II LGS AO system was generously provided by the W. M. Keck Foundation. This material is based on work supported in part by the National Science Foundation Science and Technology Center for Adaptive Optics, managed by the University of California at Santa Cruz under agreement AST 98-76783, and based on work supported in part under the auspices of the US Department of Energy, National Nuclear Security Administration, by the University of California, Lawrence Livermore National Laboratory, under contract W-7405-Eng-48. Any opinions, findings, and conclusions or recommendations expressed in this material are those of the authors and do not necessarily reflect the views of the National Science Foundation or the US Department of Energy.

The author list reflects those people directly involved in the implementation of the LGS AO system. Many individuals have contributed to the development and implementation of the Keck AO systems and laser over the years, including S. Acton, J. An, K. Avicola, J. Bell, J. Brase, F. Chaffee, J. Chock, L. Chock, R. Cohen, A. Conrad, G. Erbert, H. Friedman, J. Gathright, D. Gavel, A. Gleckler, P. Goude, T. Gregory, M. Hess, K. Ho, H. Jones, K. Kinoshita, T. Kuklo, O. Lai, W. Lupton, I. Lynn, B. Macintosh, J. Maute, C. Melcher, D. McBride, D. Medeiros, R. Mouser, C. Nance, C. Neyman, S. Olivier, T. Saloga, C. Shelton, M. Sirota, R. Sumner, K. Sweeney, K. Waltjen, J. Watson, T. Williams, N. Wong, and the entire support staff of the W. M. Keck Observatory. We would also like to express our appreciation to past and present members of our review committees and AO working groups: E. Becklin, M. Brown, G. Chanan, R. Dekany, P. Everett, R. Fugate, A. Ghez, B. Kibrick, S. Kulkarni, J. Larkin, M. Liu, T. Mast, K. Matthews, J. Nelson, D. Sandler, and M. Troy.

The data presented herein were obtained at the W. M. Keck Observatory, which is operated as a scientific partnership among the California Institute of Technology, the University of California, and the National Aeronautics and Space Administration. The Observatory was made possible by the generous financial support of the W. M. Keck Foundation. The authors wish to recognize and acknowledge the significant cultural role and reverence that the summit of Mauna Kea has always had within the Hawaiian community. We are most fortunate to have the opportunity to conduct observations from this mountain.

Footnotes

4 W. M. Keck Observatory laser guide star adaptive optics observation support Web page, http://www2.keck.hawaii.edu/optics/lgsao.

5 W. M. Keck Observatory astronomical science with adaptive optics bibliography, http://www2.keck.hawaii.edu/library/biblios/aokeck.php.

References

↑ Bouchez A. H. *et al* 2004 *Proc. SPIE* **5490** 321
Crossref

↑ Brown M. E. *et al* 2005 *ApJ* **632** L45
IOPscience (http://iopscience.iop.org/1538-4357/632/1/L45)

↑ Colavita M. M., Wizinowich P. L. and Akeson R. L. 2004 *Proc. SPIE* **5491** 454
Crossref

↑ Foy R. and Labeyrie A. 1985 *A&A* **152** L29

↑ Friedman H. W. *et al* 1998 *Proc. SPIE* **3353** 260
Crossref

↑ Gal-Yam A. *et al* 2005 *ApJ* **630** L29
IOPscience (http://iopscience.iop.org/1538-4357/630/1/L29)

↑ Ghez A. M. *et al* 2005 *ApJ* **635** 1087
IOPscience (http://iopscience.iop.org/0004-637X/635/2/1087)

↑ Graves J. E., Roddier F., Northcott M., Anuskiewicz J. and Monnet G. 1994 *Proc. SPIE* **2201** 502
Crossref

↑ Hackenberg W. *et al* 2000 *A&A* **363** 41

↑ Hayano Y. *et al* 2003 *PASP* **115** 1419
IOPscience (http://iopscience.iop.org/1538-3873/115/814/1419)

↑ Larkin J. *et al* 2003 *Proc. SPIE* **4841** 1600
Crossref

↑ Liu M. C. *et al* 2005 *ApJ* **634** 616
IOPscience (http://iopscience.iop.org/0004-637X/634/1/616)

↑ Marchis F., Descamps P., Hestroffer D. and Berthier J. 2005 *Nature* **436** 822
Crossref

↑ Max C. *et al* 1997 *Science* **277** 1649
Crossref

↑ McCullough P. R. *et al* 1995 *ApJ* **438** 394
Crossref

↑ McLean I. S. *et al* 1998 *Proc. SPIE* **3354** 566
Crossref

↑ Melbourne J. *et al* 2005 *ApJ* **625** L27
IOPscience (http://iopscience.iop.org/1538-4357/625/1/L27)

↑ Perrin M. D. *et al* 2004 *Science* **303** 1345
Crossref

↑ Rigaut F. *et al* 1998 *PASP* **110** 152
IOPscience (http://iopscience.iop.org/1538-3873/110/744/152)

↑ Rousset G. *et al* 1994 *Proc. SPIE* **2201** 1088
Crossref

↑ Stomski P., Le Mignant D., Wizinowich P., Campbell R. and Goodrich R. 2003 *Proc. SPIE* **4839** 943
Crossref

↑ Stomski P. J. and Shelton J. C. 2000 *Proc. SPIE* **4007** 608
Crossref

↑ Summers D. *et al* 2003 *Proc. SPIE* **4839** 440
Crossref

↑ 2004 *Proc. SPIE* **5490** 1117
Crossref

↑ Thompson L. and Gardner C. 1987 *Nature* **328** 229
Crossref

↑ van Dam M., Le Mignant D. and Macintosh B. 2004 *Appl. Opt.* **43** 5458
Crossref

↑ van Dam M. *et al* 2006 *PASP* **118** 310
IOPscience (http://iopscience.iop.org/1538-3873/118/840/310)

↑ Wizinowich P., Simons D., Takami H., Veillet C. and Wainscoat R. 1998 *Proc. SPIE* **3353** 290
Crossref

↑ Wizinowich P. *et al* 2000a *PASP* **112** 315
IOPscience (http://iopscience.iop.org/1538-3873/112/769/315)

↑ 2000b *Proc. SPIE* **4007** 2
Crossref

Export references: BibTeX RIS

Citations

1. Robo-AO Kepler Planetary Candidate Survey. III. Adaptive Optics Imaging of 1629 Kepler Exoplanet Candidate Host Stars
   Carl Ziegler *et al.* 2017 *The Astronomical Journal* **153** 66
   IOPscience (/1538-3881/153/2/66)

2. Probability of the Physical Association of 104 Blended Companions to Kepler Objects of Interest Using Visible and Near-infrared Adaptive Optics Photometry
   Dani Atkinson *et al.* 2017 *The Astronomical Journal* **153** 25
   IOPscience (/1538-3881/153/1/25)

3. Quasars Probing Galaxies. I. Signatures of Gas Accretion at Redshift Approximately 0.2
   Stephanie H. Ho *et al.* 2017 *The Astrophysical Journal* **835** 267
   IOPscience (/0004-637X/835/2/267)

4. First light for the sodium laser guide star adaptive optics system on the Lijiang 1.8m telescope
   Kai Wei *et al* 2016 *Research in Astronomy and Astrophysics* **16** 183
   IOPscience (/1674-4527/16/12/183)

5. MAD Adaptive Optics Imaging of High-luminosity Quasars: A Pilot Project
   E. Liuzzo *et al.* 2016 *The Astronomical Journal* **152** 38
   IOPscience (/1538-3881/152/2/38)

6. Robo-AO Kepler Planetary Candidate Survey. II. Adaptive Optics Imaging of 969 Kepler Exoplanet Candidate Host Stars
Christoph Baranec *et al.* 2016 *The Astronomical Journal* **152** 18
IOPscience (/1538-3881/152/1/18)

7. Adaptive Optics at Optical Wavelengths: Test Observations of Kyoto 3DII Connected to Subaru Telescope AO188
K. Matsubayashi *et al.* 2016 *Publications of the Astronomical Society of the Pacific* **128** 095003
IOPscience (/1538-3873/128/967/095003)

8. The Nature of Active Galactic Nuclei with Velocity Offset Emission Lines
F. Müller-Sánchez *et al.* 2016 *The Astrophysical Journal* **830** 50
IOPscience (/0004-637X/830/1/50)

9. A Search For Stellar-mass Black Holes Via Astrometric Microlensing
J. R. Lu *et al.* 2016 *The Astrophysical Journal* **830** 41
IOPscience (/0004-637X/830/1/41)

10. An Improved Distance and Mass Estimate for Sgr A* from a Multistar Orbit Analysis
A. Boehle *et al.* 2016 *The Astrophysical Journal* **830** 17
IOPscience (/0004-637X/830/1/17)

11. Multi-wavelength Lens Reconstruction of a Planck and Herschel-detected Star-bursting Galaxy
Nicholas Timmons *et al.* 2016 *The Astrophysical Journal* **829** 21
IOPscience (/0004-637X/829/1/21)

12. The Orbit of the L Dwarf + T Dwarf Spectral Binary SDSS J080531.84+481233.0
Adam J. Burgasser *et al.* 2016 *The Astrophysical Journal* **827** 25
IOPscience (/0004-637X/827/1/25)

13. The Angular Momentum Distribution and Baryon Content of Star-forming Galaxies at z ~ 1–3
A. Burkert *et al.* 2016 *The Astrophysical Journal* **826** 214
IOPscience (/0004-637X/826/2/214)

14. Four Dual AGN Candidates Observed with the VLBA
K. É. Gabányi *et al.* 2016 *The Astrophysical Journal* **826** 106
IOPscience (/0004-637X/826/2/106)

15. A Keck Adaptive Optics Survey of a Representative Sample of Gravitationally Lensed Star-forming Galaxies: High Spatial Resolution Studies of Kinematics and Metallicity Gradients
Nicha Leethochawalit *et al.* 2016 *The Astrophysical Journal* **820** 84
IOPscience (/0004-637X/820/2/84)

16. Resolving Gas Flows in the Ultraluminous Starburst IRAS 23365+3604 with Keck LGSAO/OSIRIS
Crystal L. Martin and Kurt T. Soto 2016 *The Astrophysical Journal* **819** 49

IOPscience (/0004-637X/819/1/49)

17. A Normal Supermassive Black Hole in NGC 1277
Alister W. Graham *et al.* 2016 *The Astrophysical Journal* **819** 43
IOPscience (/0004-637X/819/1/43)

18. Two Small Temperate Planets Transiting Nearby M Dwarfs in K2 Campaigns 0 and 1
Joshua E. Schlieder *et al.* 2016 *The Astrophysical Journal* **818** 87
IOPscience (/0004-637X/818/1/87)

19. Young ``Dipper" Stars in Upper Sco and Oph Observed by K2
M. Ansdell *et al.* 2016 *The Astrophysical Journal* **816** 69
IOPscience (/0004-637X/816/2/69)

20. Near-infrared Spectroscopy of 2M0441+2301 AabBab: A Quadruple System Spanning the Stellar to Planetary Mass Regimes
Brendan P. Bowler and Lynne A. Hillenbrand 2015 *The Astrophysical Journal Letters* **811** L30
IOPscience (/2041-8205/811/2/L30)

21. Radio Emission and Orbital Motion from the Close-encounter Star–Brown Dwarf Binary WISE J072003.20–084651.2
Adam J. Burgasser *et al.* 2015 *The Astronomical Journal* **150** 180
IOPscience (/1538-3881/150/6/180)

22. High Resolution Imaging of Very Low Mass Spectral Binaries: Three Resolved Systems and Detection of Orbital Motion in an L/T Transition Binary
Daniella C. Bardalez Gagliuffi *et al.* 2015 *The Astronomical Journal* **150** 163
IOPscience (/1538-3881/150/5/163)

23. WISE J072003.20-084651.2: an Old and Active M9.5 + T5 Spectral Binary 6 pc from the Sun
Adam J. Burgasser *et al.* 2015 *The Astronomical Journal* **149** 104
IOPscience (/1538-3881/149/3/104)

24. Astronomical Adaptive Optics
François Rigaut 2015 *Publications of the Astronomical Society of the Pacific* **127** 1197
IOPscience (/1538-3873/127/958/1197)

25. Photon Return On-Sky Test of Pulsed Sodium Laser Guide Star with D_{2b} Repumping
Kai Jin *et al.* 2015 *Publications of the Astronomical Society of the Pacific* **127** 749
IOPscience (/1538-3873/127/954/749)

26. Precision cosmology with time delay lenses: high resolution imaging requirements
Xiao-Lei Meng *et al* 2015 *Journal of Cosmology and Astroparticle Physics* **2015** 059
IOPscience (/1475-7516/2015/09/059)

27. Planets around Low-mass Stars (PALMS). IV. The Outer Architecture of M Dwarf Planetary Systems

Brendan P. Bowler *et al.* 2015 *The Astrophysical Journal Supplement Series* **216** 7
IOPscience (/0067-0049/216/1/7)

28. 3D Adaptive Mesh Refinement Simulations of the Gas Cloud G2 Born within the Disks of Young Stars in the Galactic Center
M. Schartmann *et al.* 2015 *The Astrophysical Journal* **811** 155
IOPscience (/0004-637X/811/2/155)

29. Characterization of the Inner Knot of the Crab: The Site of the Gamma-Ray Flares?
Alexander Rudy *et al.* 2015 *The Astrophysical Journal* **811** 24
IOPscience (/0004-637X/811/1/24)

30. Spatially Resolved Imaging and Spectroscopy of Candidate Dual Active Galactic Nuclei
R. C. McGurk *et al.* 2015 *The Astrophysical Journal* **811** 14
IOPscience (/0004-637X/811/1/14)

31. The Most Luminous Galaxies Discovered by WISE
Chao-Wei Tsai *et al.* 2015 *The Astrophysical Journal* **805** 90
IOPscience (/0004-637X/805/2/90)

32. The Mass–Luminosity Relation in the L/T Transition: Individual Dynamical Masses for the New J-band Flux Reversal Binary SDSSJ105213.51+442255.7AB
Trent J. Dupuy *et al.* 2015 *The Astrophysical Journal* **805** 56
IOPscience (/0004-637X/805/1/56)

33. Following Black Hole Scaling Relations through Gas-rich Mergers
Anne M. Medling *et al.* 2015 *The Astrophysical Journal* **803** 61
IOPscience (/0004-637X/803/2/61)

34. Discovery of a Low-luminosity, Tight Substellar Binary at the T/Y Transition
Trent J. Dupuy *et al.* 2015 *The Astrophysical Journal* **803** 102
IOPscience (/0004-637X/803/2/102)

35. Detection of Galactic Center Source G2 at 3.8 μm during Periapse Passage
G. Witzel *et al.* 2014 *The Astrophysical Journal Letters* **796** L8
IOPscience (/2041-8205/796/1/L8)

36. NEOWISE-R Observation of the Coolest Known Brown Dwarf
Edward L. Wright *et al.* 2014 *The Astronomical Journal* **148** 82
IOPscience (/1538-3881/148/5/82)

37. WISEP J061135.13–041024.0 AB: A J-band Flux Reversal Binary at the L/T Transition
Christopher R. Gelino *et al.* 2014 *The Astronomical Journal* **148** 6
IOPscience (/1538-3881/148/1/6)

38. Three New Cool Brown Dwarfs Discovered with the Wide-field Infrared Survey Explorer (WISE) and an Improved Spectrum of the Y0 Dwarf WISE J041022.71+150248.4

Michael C. Cushing *et al.* 2014 *The Astronomical Journal* **147** 113
IOPscience (/1538-3881/147/5/113)

39. Efficiency Measurements and Installation of a New Grating for the OSIRIS Spectrograph at Keck Observatory
Etsuko Mieda *et al.* 2014 *Publications of the Astronomical Society of the Pacific* **126** 250
IOPscience (/1538-3873/126/937/250)

40. Lens Models of Herschel-selected Galaxies from High-resolution Near-IR Observations
J. A. Calanog *et al.* 2014 *The Astrophysical Journal* **797** 138
IOPscience (/0004-637X/797/2/138)

41. Compact Quiescent Galaxies at Intermediate Redshifts
Li-Yen Hsu *et al.* 2014 *The Astrophysical Journal* **796** 92
IOPscience (/0004-637X/796/2/92)

42. Interferometric Follow-up of WISE Hyper-luminous Hot, Dust-obscured Galaxies
Jingwen Wu *et al.* 2014 *The Astrophysical Journal* **793** 8
IOPscience (/0004-637X/793/1/8)

43. A Continuum of H- to He-rich Tidal Disruption Candidates With a Preference for E+A Galaxies
Iair Arcavi *et al.* 2014 *The Astrophysical Journal* **793** 38
IOPscience (/0004-637X/793/1/38)

44. Wide Cool and Ultracool Companions to Nearby Stars from Pan-STARRS 1
Niall R. Deacon *et al.* 2014 *The Astrophysical Journal* **792** 119
IOPscience (/0004-637X/792/2/119)

45. New Evidence for a Substellar Luminosity Problem: Dynamical Mass for the Brown Dwarf Binary GI 417BC
Trent J. Dupuy *et al.* 2014 *The Astrophysical Journal* **790** 133
IOPscience (/0004-637X/790/2/133)

46. Constraints on the Progenitor System of the Type Ia Supernova 2014J from Pre-explosion Hubble Space Telescope Imaging
Patrick L. Kelly *et al.* 2014 *The Astrophysical Journal* **790** 3
IOPscience (/0004-637X/790/1/3)

47. Circumnuclear Molecular Gas in Megamaser Disk Galaxies NGC 4388 and NGC 1194
Jenny E. Greene *et al.* 2014 *The Astrophysical Journal* **788** 145
IOPscience (/0004-637X/788/2/145)

48. M-dwarf Rapid Rotators and the Detection of Relatively Young Multiple M-Star Systems
S. Rappaport *et al.* 2014 *The Astrophysical Journal* **788** 114
IOPscience (/0004-637X/788/2/114)

49. A Search for Companions to Brown Dwarfs in the Taurus and Chamaeleon Star-Forming Regions
K. O. Todorov *et al.* 2014 *The Astrophysical Journal* **788** 40
IOPscience (/0004-637X/788/1/40)

50. Young Star Clusters in the Circumnuclear Region of NGC 2110
Mark Durré and Jeremy Mould 2014 *The Astrophysical Journal* **784** 79
IOPscience (/0004-637X/784/1/79)

51. Stellar and Gaseous Nuclear Disks Observed in Nearby (U)LIRGs
Anne M. Medling *et al.* 2014 *The Astrophysical Journal* **784** 70
IOPscience (/0004-637X/784/1/70)

52. WISE Y Dwarfs as Probes of the Brown Dwarf-Exoplanet Connection
C. Beichman *et al.* 2014 *The Astrophysical Journal* **783** 68
IOPscience (/0004-637X/783/2/68)

53. First Faint Dual-field Off-axis Observations in Optical Long Baseline Interferometry
J. Woillez *et al.* 2014 *The Astrophysical Journal* **783** 104
IOPscience (/0004-637X/783/2/104)

54. A Magnified View of the Kinematics and Morphology of RCSGA 032727-132609: Zooming in on a Merger at z = 1.7
Eva Wuyts *et al.* 2014 *The Astrophysical Journal* **781** 61
IOPscience (/0004-637X/781/2/61)

55. A Search for Moderate-redshift Survivors from the Population of Luminous Compact Passive Galaxies at High Redshift
Alan Stockton *et al.* 2014 *The Astrophysical Journal* **780** 134
IOPscience (/0004-637X/780/2/134)

56. The Density of Mid-sized Kuiper Belt Object 2002 UX25 and the Formation of the Dwarf Planets
M. E. Brown 2013 *The Astrophysical Journal Letters* **778** L34
IOPscience (/2041-8205/778/2/L34)

57. Keck Observations of the Galactic Center Source G2: Gas Cloud or Star?
K. Phifer *et al.* 2013 *The Astrophysical Journal Letters* **773** L13
IOPscience (/2041-8205/773/1/L13)

58. A T8.5 Brown Dwarf Member of the ξ Ursae Majoris System
Edward L. Wright *et al.* 2013 *The Astronomical Journal* **145** 84
IOPscience (/1538-3881/145/3/84)

59. The Keck Interferometer
M. M. Colavita *et al.* 2013 *Publications of the Astronomical Society of the Pacific* **125** 1226
IOPscience (/1538-3873/125/932/1226)

60. Astronomical Science with Adaptive Optics at the W. M. Keck Observatory
Peter Wizinowich 2013 *Publications of the Astronomical Society of the Pacific* **125** 798
IOPscience (/1538-3873/125/929/798)

61. Millions of Multiples: Detecting and Characterizing Close-separation Binary Systems in Synoptic Sky Surveys
Emil Terziev *et al.* 2013 *The Astrophysical Journal Supplement Series* **206** 18
IOPscience (/0067-0049/206/2/18)

62. A Study of the Diverse T Dwarf Population Revealed by WISE
Gregory N. Mace *et al.* 2013 *The Astrophysical Journal Supplement Series* **205** 6
IOPscience (/0067-0049/205/1/6)

63. The Binary White Dwarf LHS 3236
Hugh C. Harris *et al.* 2013 *The Astrophysical Journal* **779** 21
IOPscience (/0004-637X/779/1/21)

64. The Circumnuclear Star Formation Environment of NGC 6946: Br γ and H2 Results from Keck Integral Field Spectroscopy
Chao-Wei Tsai *et al.* 2013 *The Astrophysical Journal* **776** 70
IOPscience (/0004-637X/776/2/70)

65. The Inner Kiloparsec of Mrk 273 with Keck Adaptive Optics
Vivian U *et al.* 2013 *The Astrophysical Journal* **775** 115
IOPscience (/0004-637X/775/2/115)

66. Proper Motions and Origins of AXP 1E 2259+586 and AXP 4U 0142+61
Shriharsh P. Tendulkar *et al.* 2013 *The Astrophysical Journal* **772** 31
IOPscience (/0004-637X/772/1/31)

67. Keck Adaptive Optics Observations of the Protostellar Disk around Radio Source I in the Orion Kleinmann-Low Nebula
Breann N. Sitarski *et al.* 2013 *The Astrophysical Journal* **770** 134
IOPscience (/0004-637X/770/2/134)

68. Mapping the Clumpy Structures within Submillimeter Galaxies Using Laser-Guide Star Adaptive Optics Spectroscopy
Karín Menéndez-Delmestre *et al.* 2013 *The Astrophysical Journal* **767** 151
IOPscience (/0004-637X/767/2/151)

69. The Origin and Evolution of Metallicity Gradients: Probing the Mode of Mass Assembly at z 2
Tucker Jones *et al.* 2013 *The Astrophysical Journal* **765** 48
IOPscience (/0004-637X/765/1/48)

70. Stellar Populations in the Central 0.5 pc of the Galaxy. I. A New Method for Constructing Luminosity Functions and Surface-density Profiles
T. Do *et al.* 2013 *The Astrophysical Journal* **764** 154

IOPscience (/0004-637X/764/2/154)

71. The Coldest Brown Dwarf (or Free-floating Planet)?: The Y Dwarf WISE 1828+2650
C. Beichman *et al.* 2013 *The Astrophysical Journal* **764** 101
IOPscience (/0004-637X/764/1/101)

72. A Radio System for Avoiding Illuminating Aircraft with a Laser Beam
W. A. Coles *et al.* 2012 *Publications of the Astronomical Society of the Pacific* **124** 42
IOPscience (/1538-3873/124/911/42)

73. The Hawaii Infrared Parallax Program. I. Ultracool Binaries and the L/T Transition
Trent J. Dupuy and Michael C. Liu 2012 *The Astrophysical Journal Supplement Series* **201** 19
IOPscience (/0067-0049/201/2/19)

74. Proper Motions and Origins of SGR 1806–20 and SGR 1900+14
Shriharsh P. Tendulkar *et al.* 2012 *The Astrophysical Journal* **761** 76
IOPscience (/0004-637X/761/1/76)

75. Two Extraordinary Substellar Binaries at the T/Y Transition and the Y-band Fluxes of the Coolest Brown Dwarfs
Michael C. Liu *et al.* 2012 *The Astrophysical Journal* **758** 57
IOPscience (/0004-637X/758/1/57)

76. Multiple Star Formation to the Bottom of the Initial Mass Function
Adam L. Kraus and Lynne A. Hillenbrand 2012 *The Astrophysical Journal* **757** 141
IOPscience (/0004-637X/757/2/141)

77. Dynamical Measurements of Black Hole Masses in Four Brightest Cluster Galaxies at 100 Mpc
Nicholas J. McConnell *et al.* 2012 *The Astrophysical Journal* **756** 179
IOPscience (/0004-637X/756/2/179)

78. A Detailed Gravitational Lens Model Based on Submillimeter Array and Keck Adaptive Optics Imaging of a Herschel-ATLAS Submillimeter Galaxy at z = 4.243
R. S. Bussmann *et al.* 2012 *The Astrophysical Journal* **756** 134
IOPscience (/0004-637X/756/2/134)

79. The First Hyper-luminous Infrared Galaxy Discovered by WISE
Peter R. M. Eisenhardt *et al.* 2012 *The Astrophysical Journal* **755** 173
IOPscience (/0004-637X/755/2/173)

80. A Comprehensive View of a Strongly Lensed Planck-Associated Submillimeter Galaxy
Hai Fu *et al.* 2012 *The Astrophysical Journal* **753** 134
IOPscience (/0004-637X/753/2/134)

81. A Stellar Dynamical Mass Measurement of the Black Hole in NGC 3998 from Keck Adaptive Optics Observations
Jonelle L. Walsh *et al.* 2012 *The Astrophysical Journal* **753** 79

IOPscience (/0004-637X/753/1/79)

82. Proper Motions of the Arches Cluster with Keck Laser Guide Star Adaptive Optics: The First Kinematic Mass Measurement of the Arches
W. I. Clarkson *et al.* 2012 *The Astrophysical Journal* **751** 132
IOPscience (/0004-637X/751/2/132)

83. Rotational Velocities of Individual Components in Very Low Mass Binaries
Q. M. Konopacky *et al.* 2012 *The Astrophysical Journal* **750** 79
IOPscience (/0004-637X/750/1/79)

84. The Nature of Double-peaked [O III] Active Galactic Nuclei
Hai Fu *et al.* 2012 *The Astrophysical Journal* **745** 67
IOPscience (/0004-637X/745/1/67)

85. Resolved Spectroscopy of a Brown Dwarf Binary at the T Dwarf/Y Dwarf Transition
Adam J. Burgasser *et al.* 2012 *The Astrophysical Journal* **745** 26
IOPscience (/0004-637X/745/1/26)

86. Eruptive Variable Stars and Outflows in Serpens NW
Klaus W. Hodapp *et al.* 2012 *The Astrophysical Journal* **744** 56
IOPscience (/0004-637X/744/1/56)

87. The Progenitor of Supernova 2011dh/PTF11eon in Messier 51
Schuyler D. Van Dyk *et al.* 2011 *The Astrophysical Journal Letters* **741** L28
IOPscience (/2041-8205/741/2/L28)

88. A Kiloparsec-scale Binary Active Galactic Nucleus Confirmed by the Expanded Very Large Array
Hai Fu *et al.* 2011 *The Astrophysical Journal Letters* **740** L44
IOPscience (/2041-8205/740/2/L44)

89. Spatially Resolved Spectroscopy of SDSS J0952+2552: A Confirmed Dual Active Galactic Nucleus
R. C. McGurk *et al.* 2011 *The Astrophysical Journal Letters* **738** L2
IOPscience (/2041-8205/738/1/L2)

90. Discovery of a Multiply Lensed Submillimeter Galaxy in Early HerMES Herschel/SPIRE Data
A. Conley *et al.* 2011 *The Astrophysical Journal Letters* **732** L35
IOPscience (/2041-8205/732/2/L35)

91. WISE Brown Dwarf Binaries: The Discovery of a T5+T5 and a T8.5+T9 System
Christopher R. Gelino *et al.* 2011 *The Astronomical Journal* **142** 57
IOPscience (/1538-3881/142/2/57)

92. The First Hundred Brown Dwarfs Discovered by the Wide-field Infrared Survey Explorer (WISE)
J. Davy Kirkpatrick *et al.* 2011 *The Astrophysical Journal Supplement Series* **197** 19
IOPscience (/0067-0049/197/2/19)

93. The Discovery of Y Dwarfs using Data from the Wide-field Infrared Survey Explorer (WISE)
Michael C. Cushing *et al.* 2011 *The Astrophysical Journal* **743** 50
IOPscience (/0004-637X/743/1/50)

94. Mass of the Southern Black Hole in NGC 6240 from Laser Guide Star Adaptive Optics
Anne M. Medling *et al.* 2011 *The Astrophysical Journal* **743** 32
IOPscience (/0004-637X/743/1/32)

95. CFBDSIR J1458+1013B: A Very Cold (>T10) Brown Dwarf in a Binary System
Michael C. Liu *et al.* 2011 *The Astrophysical Journal* **740** 108
IOPscience (/0004-637X/740/2/108)

96. Outflows from Active Galactic Nuclei: Kinematics of the Narrow-line and Coronal-line Regions in Seyfert Galaxies
F. Müller-Sánchez *et al.* 2011 *The Astrophysical Journal* **739** 69
IOPscience (/0004-637X/739/2/69)

97. The Hyperactive L Dwarf 2MASS J13153094−2649513: Continued Emission and a Brown Dwarf Companion
Adam J. Burgasser *et al.* 2011 *The Astrophysical Journal* **739** 49
IOPscience (/0004-637X/739/1/49)

98. Discovery of Two L and T Binaries with Wide Separations and Peculiar Photometric Properties
Étienne Artigau *et al.* 2011 *The Astrophysical Journal* **739** 48
IOPscience (/0004-637X/739/1/48)

99. Adaptive Optics Imaging of Quasi-stellar Objects with Double-peaked Narrow Lines: Are They Dual Active Galactic Nuclei?
D. J. Rosario *et al.* 2011 *The Astrophysical Journal* **739** 44
IOPscience (/0004-637X/739/1/44)

100. The Discovery and Nature of the Optical Transient CSS100217:102913+404220
A. J. Drake *et al.* 2011 *The Astrophysical Journal* **735** 106
IOPscience (/0004-637X/735/2/106)

101. Mergers in Double-peaked [O III] Active Galactic Nuclei
Hai Fu *et al.* 2011 *The Astrophysical Journal* **733** 103
IOPscience (/0004-637X/733/2/103)

102. The Black Hole Mass in the Brightest Cluster Galaxy NGC 6086
Nicholas J. McConnell *et al.* 2011 *The Astrophysical Journal* **728** 100
IOPscience (/0004-637X/728/2/100)

103. Spatially Resolving the HK Tau B Edge-on Disk from 1.2 to 4.7 μm: A Unique Scattered Light Disk
C. McCabe *et al.* 2011 *The Astrophysical Journal* **727** 90
IOPscience (/0004-637X/727/2/90)

104. Searching for Young M Dwarfs with GALEX
Evgenya L. Shkolnik *et al.* 2011 *The Astrophysical Journal* **727** 6
IOPscience (/0004-637X/727/1/6)

105. The 2008 Outburst in the Young Stellar System Z CMa: The First Detection of Twin Jets
E. T. Whelan *et al.* 2010 *The Astrophysical Journal Letters* **720** L119
IOPscience (/2041-8205/720/1/L119)

106. Two Moderate-redshift Analogs to Compact Massive Early-type Galaxies at High Redshifts
Alan Stockton *et al.* 2010 *The Astrophysical Journal Letters* **709** L58
IOPscience (/2041-8205/709/1/L58)

107. Unveiling the Origin of Grb 090709A: Lack of Periodicity in a Reddened Cosmological Long-Duration Gamma-Ray Burst
S. B. Cenko *et al.* 2010 *The Astronomical Journal* **140** 224
IOPscience (/1538-3881/140/1/224)

108. 2MASS J20261584–2943124: an Unresolved L0.5 + T6 Spectral Binary
Christopher R. Gelino and Adam J. Burgasser 2010 *The Astronomical Journal* **140** 110
IOPscience (/1538-3881/140/1/110)

109. Ultracool Field Brown Dwarf Candidates Selected at 4.5 μm
Peter R. M. Eisenhardt *et al.* 2010 *The Astronomical Journal* **139** 2455
IOPscience (/1538-3881/139/6/2455)

110. New Observations of the Very Luminous Supernova 2006gy: Evidence for Echoes
A. A. Miller *et al.* 2010 *The Astronomical Journal* **139** 2218
IOPscience (/1538-3881/139/6/2218)

111. Discovery of Precursor Luminous Blue Variable Outbursts in Two Recent Optical Transients: The Fitfully Variable Missing Links UGC 2773-OT and SN 2009ip
Nathan Smith *et al.* 2010 *The Astronomical Journal* **139** 1451
IOPscience (/1538-3881/139/4/1451)

112. Adaptive Optics Imaging of a Massive Galaxy Associated With a Metal-Rich Absorber
Mark R. Chun *et al.* 2010 *The Astronomical Journal* **139** 296
IOPscience (/1538-3881/139/1/296)

113. Integrated Laboratory Demonstrations of Multi-Object Adaptive Optics on a Simulated 10 Meter Telescope at Visible Wavelengths
S. Mark Ammons *et al.* 2010 *Publications of the Astronomical Society of the Pacific* **122** 573
IOPscience (/1538-3873/122/891/573)

114. The Kinematics of Ionized Gas in Lyman-break Analogs at z ~ 0.2
Thiago S. Gonçalves *et al.* 2010 *The Astrophysical Journal* **724** 1373
IOPscience (/0004-637X/724/2/1373)

115. Discovery of a Highly Unequal-mass Binary T Dwarf with Keck Laser Guide Star Adaptive Optics: A Coevality Test of Substellar Theoretical Models and Effective Temperatures
Michael C. Liu *et al.* 2010 *The Astrophysical Journal* **722** 311
IOPscience (/0004-637X/722/1/311)

116. Studying the Physical Diversity of Late-M Dwarfs with Dynamical Masses
Trent J. Dupuy *et al.* 2010 *The Astrophysical Journal* **721** 1725
IOPscience (/0004-637X/721/2/1725)

117. The High-order Multiplicity of Unusually Wide M Dwarf Binaries: Eleven New Triple and Quadruple Systems
N. M. Law *et al.* 2010 *The Astrophysical Journal* **720** 1727
IOPscience (/0004-637X/720/2/1727)

118. Disks in the Arches Cluster—Survival in a Starburst Environment
A. Stolte *et al.* 2010 *The Astrophysical Journal* **718** 810
IOPscience (/0004-637X/718/2/810)

119. The Lick AGN Monitoring Project: The M BH-σ* Relation for Reverberation-mapped Active Galaxies
Jong-Hak Woo *et al.* 2010 *The Astrophysical Journal* **716** 269
IOPscience (/0004-637X/716/1/269)

120. Discovery of A Young L Dwarf Binary, SDSS J224953.47+004404.6AB
K. N. Allers *et al.* 2010 *The Astrophysical Journal* **715** 561
IOPscience (/0004-637X/715/1/561)

121. Panchromatic Observations and Modeling of the HV Tau C Edge-on Disk
G. Duchêne *et al.* 2010 *The Astrophysical Journal* **712** 112
IOPscience (/0004-637X/712/1/112)

122. The Presence of Weak Active Galactic Nuclei in High Redshift Star-forming Galaxies
Shelley A. Wright *et al.* 2010 *The Astrophysical Journal* **711** 1291
IOPscience (/0004-637X/711/2/1291)

123. High-precision Dynamical Masses of Very Low Mass Binaries
Q. M. Konopacky *et al.* 2010 *The Astrophysical Journal* **711** 1087
IOPscience (/0004-637X/711/2/1087)

124. An OSIRIS Study of the Gas Kinematics in a Sample of UV-Selected Galaxies: Evidence of "Hot and Bothered" Starbursts in the Local Universe
Antara R. Basu-Zych *et al.* 2009 *The Astrophysical Journal Letters* **699** L118
IOPscience (/1538-4357/699/2/L118)

125. The Distance and Morphology of V723 Cassiopeiae (Nova Cassiopeia 1995)
J. E. Lyke and R. D. Campbell 2009 *The Astronomical Journal* **138** 1090
IOPscience (/1538-3881/138/4/1090)

126. High-Redshift Dust Obscured Galaxies: A Morphology-Spectral Energy Distribution Connection Revealed by Keck Adaptive Optics
J. Melbourne *et al.* 2009 *The Astronomical Journal* **137** 4854
IOPscience (/1538-3881/137/6/4854)

127. Precision Astrometry With Adaptive Optics
P. B. Cameron *et al.* 2009 *The Astronomical Journal* **137** 83
IOPscience (/1538-3881/137/1/83)

128. Spatially Resolved Stellar Populations of Eight Goods-South Active Galactic Nuclei at z ~ 1
S. Mark Ammons *et al.* 2009 *The Astronomical Journal* **137** 470
IOPscience (/1538-3881/137/1/470)

129. UnISIS: Laser Guide Star and Natural Guide Star Adaptive Optics System
Laird A. Thompson *et al.* 2009 *Publications of the Astronomical Society of the Pacific* **121** 498
IOPscience (/1538-3873/121/879/498)

130. Dynamical Mass of the M8+M8 Binary 2MASS J22062280 – 2047058AB
Trent J. Dupuy *et al.* 2009 *The Astrophysical Journal* **706** 328
IOPscience (/0004-637X/706/1/328)

131. Unusually Wide Binaries: Are They Wide or Unusual?
Adam L. Kraus and Lynne A. Hillenbrand 2009 *The Astrophysical Journal* **703** 1511
IOPscience (/0004-637X/703/2/1511)

132. High Angular Resolution Integral-Field Spectroscopy of the Galaxy's Nuclear Cluster: A Missing Stellar Cusp?
T. Do *et al.* 2009 *The Astrophysical Journal* **703** 1323
IOPscience (/0004-637X/703/2/1323)

133. An Imaging and Spectroscopic Study of Four Strong Mg II Absorbers Revealed by GRB 060418
L. K. Pollack *et al.* 2009 *The Astrophysical Journal* **701** 1605
IOPscience (/0004-637X/701/2/1605)

134. Dynamics of Galactic Disks and Mergers at z ~ 1.6: Spatially Resolved Spectroscopy with Keck Laser Guide Star Adaptive Optics
Shelley A. Wright *et al.* 2009 *The Astrophysical Journal* **699** 421
IOPscience (/0004-637X/699/1/421)

135. Keck Laser Guide Star Adaptive Optics Monitoring of the M8+L7 Binary LHS 2397aAB: First Dynamical Mass Benchmark at the L/T Transition
Trent J. Dupuy *et al.* 2009 *The Astrophysical Journal* **699** 168
IOPscience (/0004-637X/699/1/168)

136. 2MASS 22344161+4041387AB: A Wide, Young, Accreting, Low-Mass Binary in the LkHα233 Group

K. N. Allers *et al.* 2009 *The Astrophysical Journal* **697** 824
IOPscience (/0004-637X/697/1/824)

137. The Role of Molecular Gas in Obscuring Seyfert Active Galactic Nuclei
E. K. S. Hicks *et al.* 2009 *The Astrophysical Journal* **696** 448
IOPscience (/0004-637X/696/1/448)

138. A Near-Infrared Variability Study of the Galactic Black Hole: A Red Noise Source with NO Detected Periodicity
T. Do *et al.* 2009 *The Astrophysical Journal* **691** 1021
IOPscience (/0004-637X/691/2/1021)

139. A Disk of Young Stars at the Galactic Center as Determined by Individual Stellar Orbits
J. R. Lu *et al.* 2009 *The Astrophysical Journal* **690** 1463
IOPscience (/0004-637X/690/2/1463)

140. Testing for periodicities in near-IR light curves of Sgr A*
Tuan Do *et al* 2008 *Journal of Physics: Conference Series* **131** 012003
IOPscience (/1742-6596/131/1/012003)

141. CATS: Optical to Near-Infrared Colors of the Bulge and Disk of Two z = 0.7 Galaxies Using Hubble Space Telescope and Keck Laser Adaptive Optics Imaging
E. Steinbring *et al.* 2008 *The Astronomical Journal* **136** 1523
IOPscience (/1538-3881/136/4/1523)

142. An Upper Mass Limit on a Red Supergiant Progenitor for the Type II-Plateau Supernova SN 2006my
Douglas C. Leonard *et al.* 2008 *Publications of the Astronomical Society of the Pacific* **120** 1259
IOPscience (/1538-3873/120/874/1259)

143. Measuring Distance and Properties of the Milky Way's Central Supermassive Black Hole with Stellar Orbits
A. M. Ghez *et al.* 2008 *The Astrophysical Journal* **689** 1044
IOPscience (/0004-637X/689/2/1044)

144. Keck Laser Guide Star Adaptive Optics Monitoring of 2MASS J15344984–2952274AB: First Dynamical Mass Determination of a Binary T Dwarf
Michael C. Liu *et al.* 2008 *The Astrophysical Journal* **689** 436
IOPscience (/0004-637X/689/1/436)

145. Late-Time Observations of SN 2006gy: Still Going Strong
Nathan Smith *et al.* 2008 *The Astrophysical Journal* **686** 485
IOPscience (/0004-637X/686/1/485)

146. HN Peg B: A Test of Models of the L to T Dwarf Transition
S. K. Leggett *et al.* 2008 *The Astrophysical Journal* **682** 1256

IOPscience (/0004-637X/682/2/1256)

147. Subtle Signatures of Multiplicity in Late-type Dwarf Spectra: The Unresolved M8.5 + T5 Binary 2MASS J03202839–0446358
Adam J. Burgasser *et al.* 2008 *The Astrophysical Journal* **681** 579
IOPscience (/0004-637X/681/1/579)

148. Near-Infrared and X-Ray Observations of the Enigmatic G70.7+1.2
P. B. Cameron and S. R. Kulkarni 2007 *The Astrophysical Journal Letters* **665** L135
IOPscience (/1538-4357/665/2/L135)

149. Rest-Frame R-band Light Curve of a z ~ 1.3 Supernova Obtained with Keck Laser Adaptive Optics
J. Melbourne *et al.* 2007 *The Astronomical Journal* **133** 2709
IOPscience (/1538-3881/133/6/2709)

150. Discovery of a 66 mas Ultracool Binary with Laser Guide Star Adaptive Optics
Nick Siegler *et al.* 2007 *The Astronomical Journal* **133** 2320
IOPscience (/1538-3881/133/5/2320)

151. Measurements of Mesospheric Sodium Abundance above the Hawaiian Islands
Lewis C. Roberts Jr. *et al.* 2007 *Publications of the Astronomical Society of the Pacific* **119** 787
IOPscience (/1538-3873/119/857/787)

152. Laser Guide Star Adaptive Optics Integral Field Spectroscopy of a Tightly Collimated Bipolar Jet from the Herbig Ae Star LkHα 233
Marshall D. Perrin and James R. Graham 2007 *The Astrophysical Journal* **670** 499
IOPscience (/0004-637X/670/1/499)

153. Integral Field Spectroscopy of High-Redshift Star-forming Galaxies with Laser-guided Adaptive Optics: Evidence for Dispersion-dominated Kinematics
David R. Law *et al.* 2007 *The Astrophysical Journal* **669** 929
IOPscience (/0004-637X/669/2/929)

154. A Constant Spectral Index for Sagittarius A* during Infrared/X-Ray Intensity Variations
S. D. Hornstein *et al.* 2007 *The Astrophysical Journal* **667** 900
IOPscience (/0004-637X/667/2/900)

155. USco J1606-1935: An Unusually Wide Low-Mass Triple System?
Adam L. Kraus and Lynne A. Hillenbrand 2007 *The Astrophysical Journal* **664** 1167
IOPscience (/0004-637X/664/2/1167)

156. Imaging of the Stellar Population of IC 10 with Laser Guide Star Adaptive Optics and the Hubble Space Telescope
William D. Vacca *et al.* 2007 *The Astrophysical Journal* **662** 272
IOPscience (/0004-637X/662/1/272)

157. The Wide Brown Dwarf Binary Oph 1622–2405 and Discovery of a Wide, Low-Mass Binary in Ophiuchus (Oph 1623–2402): A New Class of Young Evaporating Wide Binaries?
Laird M. Close *et al.* 2007 *The Astrophysical Journal* **660** 1492
IOPscience (/0004-637X/660/2/1492)

158. Integral Field Spectroscopy of a Candidate Disk Galaxy at z ~ 1.5 Using Laser Guide Star Adaptive Optics
S. A. Wright *et al.* 2007 *The Astrophysical Journal* **658** 78
IOPscience (/0004-637X/658/1/78)

159. On the Progenitor of SN 2005gl and the Nature of Type IIn Supernovae
Avishay Gal-Yam *et al.* 2007 *The Astrophysical Journal* **656** 372
IOPscience (/0004-637X/656/1/372)

160. The W. M. Keck Observatory Laser Guide Star Adaptive Optics System: Performance Characterization
Marcos A. van Dam *et al.* 2006 *Publications of the Astronomical Society of the Pacific* **118** 310
IOPscience (/1538-3873/118/840/310)